Memoirs of the Faculty of Science, Kyoto University, Series of Physics, Astrophysics, Geophysics and Chemistry, Vol. XXXIX, No. 3, Article 2, 1996

Search for the H Dibaryon via (K^-, K^+) Reactions with Hybrid System of Spectrometer and Scintillating Fiber Target

By

Satoru YAMASHITA

Department of Physics, Faculty of Science, Kyoto University
Kyoto 606-01, Japan

(Received November 20, 1995)

Abstract

An experiment to search for the H dibaryon with $S = -2$ has been carried out using 1.66-GeV/c K^- beam at the KEK-PS. The H dibaryon was studied in the direct process, $K^- + {}^{12}C \rightarrow K^+ + H + X$. A new type of visual live target consisted of plastic scintillating fibers together with a high momentum-resolution spectrometer have been used.

The H dibaryon produced through the direct process has been studied by means of the analysis of the K^+ momentum spectrum with the help of the data of the fiber target. No evidence of the H production has been observed. The upper limit of the production cross section of the H has been obtained to be from 43 nb/sr to 73 nb/sr in the forward scattering angle of the K^+ at 90% confidence level in the mass region of the H from 1850 to 2150 MeV/c^2. The upper limit for the production of H with higher mass range up to 2230 MeV/c^2 has been also obtained to be from 80 nb/sr to 2 μb/sr for the first time.

1 Introduction

Hadrons are described as composite particles of several constituent quarks. In the naive quark model, baryons and mesons are described as composites of three quarks (q^3) and a quark-antiquark pair ($q\bar{q}$), respectively. An extension leads the possible existence of exotic multi-quark states such as $qq\bar{q}\bar{q}$, $qqqq\bar{q}$, or six-quark states (dibaryon). In 1977, Jaffe proposed the possible existence of a dibaryon comprising two up (u), two down (d), and two strange (s) quarks confined in a single hadronic "bag", and labeled this state as the "H particle" (H)[1]. The predicted quantum number is $J^{PC} = 0^{++}$, $I = 0$, $S = -2$, and $B = 2$. It constitutes the most symmetric six-quark color-spin configuration. The symmetry results in a maximally attractive color-magnetic interaction which is considered to be responsible for the hyperfine mass splitting of baryons such as the $N - \Delta$ mass difference.

The color-magnetic term E_m due to the gluon exchange between quarks is expressed in case of a particle having N quarks and no antiquarks as:

$$E_m = [8N - \frac{1}{2} C_6 + \frac{4}{3} J\ (J+1)]\ \bar{M}, \tag{1}$$

where C_6 is the eigenvalue of the color-spin Casimir operator and $\bar{M}$ is an average

interaction strength [1]. With the most symmetric color-spin configuration, hence flavor-singlet because of Pauli's principle, C_6 takes the highest number, 144, which results in the state having the largest downward shift in the mass. Note that the flavor-singlet configuration is constructed from six quarks only in the case of two u, two d and two s quarks. Therefore, as Jaffe suggested, the H plays a special role among six-quark configurations.

The mass of the H which Jaffe predicted originally using the MIT bag model was 2150 MeV/c^2, about 80 MeV/c^2 below that of the lowest lying baryon-baryon system with S$=-2$, that is, 2Λ. Thus the H would be stable against strong decays. Since then, over 15 years, this exciting prospect has spurred many physicists to considerable efforts both in experimental and theoretical investigations on the H dibaryon.

Within the context of the MIT bag model, several calculations have been made, including the center-of-mass motion or pion cloud corrections [2,3,4,5]. Predictions have been made with other models such as the Skyrme model [6], quark cluster models [7,8,9] and also the lattice QCD [10,11]. The predicted mass ranges from that of two nucleons to that of two Λ, and also to the unbound region.

An experiment searching for the H was done at BNL by looking for the reaction, $p + p \rightarrow H + K^+ + K^+$ [12]. However, the sensitivity was two order of magnitude lower than the expected production cross section.

The existence of the H with lower mass than that of two nucleons is denied in the analysis of an experiment [13] searching for the following processes:

$$\begin{array}{ll} {}^{A}_{Z}N \rightarrow {}^{A-2}_{Z-1}N + H + \beta^+ + \nu & \text{for } {}^{2}\text{H and } {}^{127}\text{I} \\ {}^{A}_{Z}N \rightarrow {}^{A-2}_{Z}N + H + \gamma & \text{for } {}^{72}\text{Ge, } {}^{70}\text{Ge and } {}^{10}\text{Be,} \end{array} \tag{2}$$

where ${}^{A}_{Z}N$ represents a nucleus with atomic number A and charge Z.

At KEK, an experiment to search for the H and/or double hypernuclei was carried out by means of an emulsion-counter hybrid technique (KEK-E176 [14]). A study was made on the direct production of the H via (K^-,K^+) reactions in emulsion:

$$K^- + (pp) \rightarrow H + K^+, \tag{3}$$

where (pp) is a proton-pair in a nucleus [14]. If the H mass is low, the H production is discriminated from the quasi-free Ξ^- production, $K^- + (p) \rightarrow K^+ + \Xi^-$, because of the high momentum of K^+. The K^+ momentum spectrum was studied to search for the H in the mass range of 1900 to 2160 MeV/c^2, however, no signal was seen. The upper limit on the production cross section was found to be $0.2 \sim 0.6\%$ of the quasi-free Ξ^- production (90% C.L.), which was comparable to the expected value [40].

They reported also several candidates of the double hypernuclei [15] which put an indirect constraint on the lower limit of the possible mass of H to be $2M_\Lambda - B_{\Lambda\Lambda}$ [16], where $B_{\Lambda\Lambda}$ is the binding energy of two Λ hyperons in the nucleus[1]. One of

[1] Double hypernuclei were reported for the first time over twenty years ago [17, 18] as the events with sequential decays in emulsion, although tagging for $S = -2$ was not made.

the candidates has been assigned as ${}^{10}_{\Lambda\Lambda}$Be or ${}^{13}_{\Lambda\Lambda}$B with the binding energy of 8.5 ± 0.7 MeV or 27.6 ± 0.7 MeV, respectively. If the interpretation is correct, the allowed mass region of the bound H is from 2203 MeV/c^2 to 2230 MeV/c^2 [19].

A candidate of the H was reported in the analysis of photographs of a propane bubble chamber at Dubna. They applied a kinematical fit on the tracks in the photograph and found an event which was translated as a possible decay of the H into $\Sigma^- p$. The mass of the H was assigned as 2173.9 ± 1.3 MeV [20], although the decay of the Σ^- from the H-decay was not observed in this event.

An experiment is in progress at BNL (BNL-E813 [21,22]) searching for the H via capture processes of Ξ^- in a deuterium-atom. The H dibaryon has been looked for in the missing-mass spectrum of the reaction:

$$(\Xi^- d)_{atom} \rightarrow n + H, \tag{4}$$

by means of the measurement of the neutron energy.

Even though above mentioned several experiments have given a lot of information on the subject, the situation is still controversial regarding the existence of H dibaryon. An experiment with enough sensitivity to search for the H dibaryon has been awaited to solve the problem. In order to arrive at the best solution for the problem, it is very important to identify the production of a particle or particles with S $=-2$ as well as to carry out the experiment with better statistics.

The observation of the vicinity of the (K^-,K^+) reaction vertex with a visual detector is advantageous in the H search, since such a detector is useful not only to confirm the (K^-,K^+) reaction but also to follow up the tracks of reaction products. Although experiments using the emulsion target provide us information on the fine structure at the interaction vertex as well as on the decay process of produced particles, only the small region of the order of 100 μm around the vertex can be studied. Also the flux of the beam is limited to avoid overlaps of many events. The situation is similar in experiments using bubble chambers. This is due to the fact that those visual detectors are not triggerable devices. Therefore, the "triggerable active target" with a large fiducial volume, which can serve as both a production target and a triggerable vertex detector, had been desired.

We performed an experiment at the KEK Proton Synchrotron (KEK-PS) to search for the H dibaryon with the (K^-,K^+) reaction. A separated K^--beam of the momentum 1.66 GeV/c at the K2 beam line was used. The experiment was executed using a hybrid system with a high resolution spectrometer for (K^-,K^+) reactions and a newly developed "triggerable active target". The target consisted of thin scintillating fibers (SCIFI-target) of about one liter. In the target, we got the three-dimensional view of tracks of charged particles in the vicinity of the reaction vertex. Image intensifier tubes (IIT) and charge-coupled-device cameras (CCD camera) enabled us to read out the tracks in the SCIFI-target with a position resolution of about 300 μm. The IITs were triggered by gate pulses using information from the counters in the spectrometer.

We studied the H production by means of two methods. One of them is the measurement of K^+ produced in the process, $K^- + {}^{12}C \rightarrow K^+ + H + X$. In this method the observation of K^+ with higher momentum than that in the quasi-free Ξ^- production is the signature of the H production.

The other one is the detection of the H which is produced in the two step reactions : $K^- + {}^{12}C \rightarrow K^+ + \Xi^- + X$, then $(\Xi^-\text{-C})_{atom} \rightarrow H + X$. In this case, the identification of the decay $H \rightarrow \Sigma^- p$ in the SCIFI-target is the signature of the H production.

In this paper we focus on the H search by means of the former method.

In the (K^-,K^+) reactions on carbon with our beam energy, the quasi-free Ξ^- production process is dominant in the K^+ momentum range above 1.0 GeV/c and about 20 % of the Ξ^-'s are absorbed in the production nuclei. According to Aerts and Dover [23], the H is produced in the reaction, $K^- + C \rightarrow K^+ + H + X$, through a fusion process of a Ξ^-, which is produced in the quasi-free (K^-,K^+) reaction on a proton in ^{12}C, and a proton in the same nuclei(see Fig 1). If the mass of the H is lower than that of $\Xi^- p$, the H production is identified by means of the observation of K^+ in the higher momentum range where the quasi-free Ξ^- production is not allowed kinematically.

In this experiment the precise measurement of the K^+ momentum is of vital importance. In addition, information on the three-dimensional track data in the SCIFI-target is useful to identify the (K^-,K^+) reactions and the produced particles in the reactions.

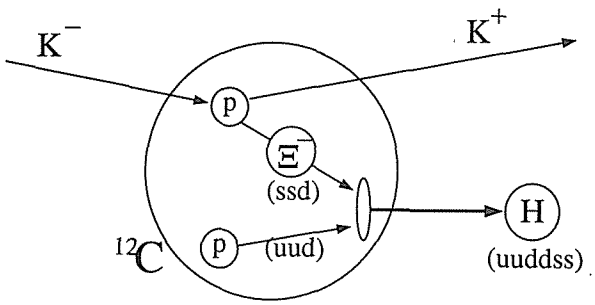

Fig. 1. Production scheme of H through the direct process in carbon, $K^- + C \rightarrow K^+ + H + X$.

2 Experimental Procedure

The experiment was carried out using the K2 beam line which delivered 1.66-GeV/c K^- beam with a typical K/π ratio of 1/4. The typical intensity of K^- was 10^4/sec. We constructed a high-resolution spectrometer for the detection of K^+. We developed also a triggerable active target made of scintillating fibers (SCIFI) in which the tracks of the reaction products as well as the incident K^- and the scattered K^+

were observed. It was the first attempt to employ scintillating fibers as a three-dimensional tracking device in the particle and/or nuclear physics.

The search for the H through the direct process was performed by the analysis of the momentum spectrum of the scattered K^+'s. A signature of the H production was the detection of a high momentum K^+ appeared above the region where the quasi-free Ξ^- production was kinematically allowed.

The measurement of the K^+ in the production angle close to 0 degree is essential to study the direct production of the H, since the momentum transfer from the incident K^- to the produced virtual Ξ^- should be small so that the virtual Ξ^- and a proton in the same nucleus fuse into an H dibaryon. The acceptance of the K^+ should then be optimized for the momentum range higher than 1.1 GeV/c. The momentum resolution is also very important in the case of higher H mass, since the momentum of K^+ in the direct process overlaps with that from the quasi-free Ξ^- production, if the resolution is not sufficient. The discrimination of the K^+ from other particles is indispensable. For this purpose, longer flight length in the spectrometer is preferable in order to measure the flight time precisely, even it is limited due to the short decay length of K^+ ($c\tau = 3.709$ m).

The schematic view of the spectrometer is shown in Fig.2. The spectrometer consisted of a dipole magnet with the field integral of 1.1 Tm, drift chambers including a cylindrical drift chamber (CDC) which surrounded the target, a silica aerogel Čerenkov counter and TOF hodoscopes. The angular acceptance of the spectrometer was about 0.09 sr with the central production angle of 0 degree. The acceptance was optimized for scattered particles of 1.2 GeV/c. In order to get a good momentum resolution, relatively dense material such as the aerogel Čerenkov counter was located downstream the last tracking chamber.

At the center of the CDC, the SCIFI-target system was installed. The plastic scintillating fibers, whose cross section had the dimension of 500 μm $\times$ 500 μm, were bundled into a block target of about one liter [25,26]. The fiber sheets were stacked in X and Y directions alternately as shown in Fig.3 to obtain the three-dimensional information of tracks. We used image intensifier tube (IIT) and CCD cameras to read out the image of the tracks.

Since the speed of the online data-taking of the data of the SCIFI-target was limited by the read-out cycle of the CCD cameras, trigger selection for the IITs with signals from the counter system played an essential role. The events of (K^-,K^+) reactions were selected from those of other reactions such as (K^-, p) reactions by calculating the mass of the scattered particles using information from the trigger counters especially with the fast-encoded time-of-flight value. The signals of the selected events were used to gate the IIT as the second-level trigger.

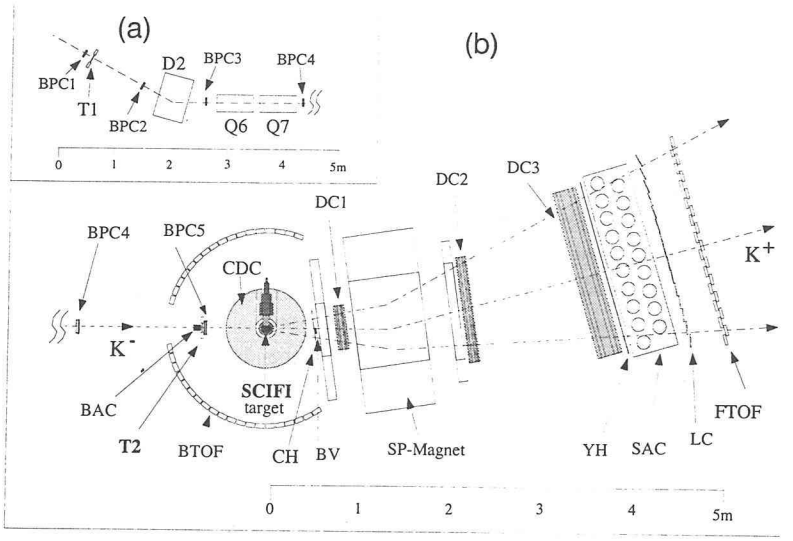

Fig. 2. Experimental setup. (a) Detectors and beam-line elements upstream the target region. (b) K^+ tagging spectrometer and the SCIFI-target.

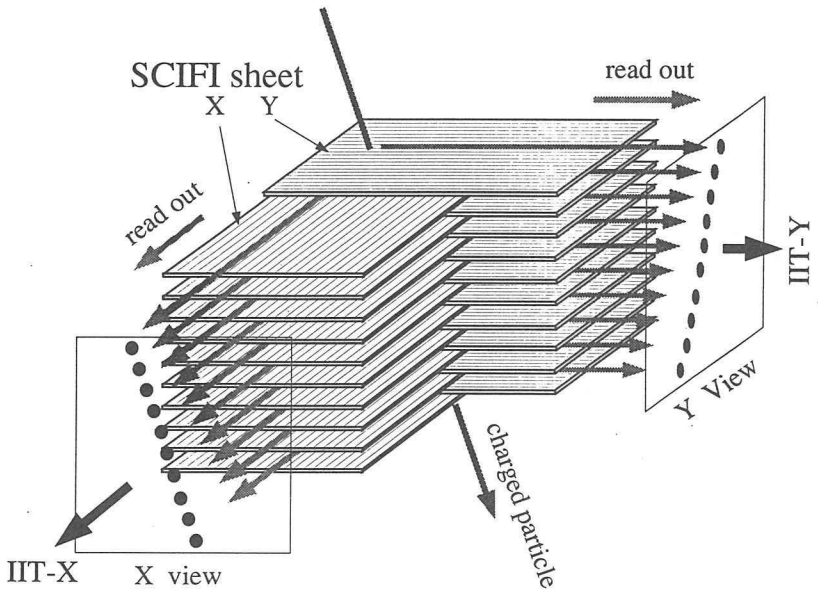

Fig. 3. Schematic view of the SCIFI-target.

2.1 Beam

2.1.1 K2 Beam Line

We used the secondary beam produced by primary protons from the KEK 12-GeV Proton Synchrotron (PS) on the production target of platinum having a size of 6 mm wide, 3 mm thick and 60 mm long. The protons were extracted from the PS in the "slow extraction" mode for the duration of about 2 sec (spill). The duty factor was about 50%. Typically, 2.1×10^{12} protons per spill were transported to the primary targetting point.

Figure 4 shows a schematic view of the K2 beam-line. The beam line was designed to serve mainly separated kaons in the momentum range between 1.0 and 2.0 GeV/c [31]. The K2 beam line consisted of two dipole magnets (D1 and D2), six quadrupole magnets (Q1,Q2,Q3,Q4,Q6 and Q7), a pair of correction magnets (CM) and an electrostatic mass separator with the length of 6 m. The total length of the beam line from the production target to the final focal point, where the SCIFI-target was placed, was about 25.8 m. The production angle at the primary target was 0°. The bending angles of D1 and D2 along the central orbit were 23° and 15°, respectively.

Tuning the electrostatic mass separator and the correction magnets for K^-, the effective angular deflection ($\Delta\theta$) of the unwanted particles such as e^-, π^- or $\bar{p}$ by the electrostatic separator is given as :

$$\Delta\theta = \frac{eEL}{pc}\left(\frac{1}{\beta_{K^-}} - \frac{1}{\beta_{BG}}\right) \simeq \frac{eEL(M_{K^-}^2 - M_{BG}^2)}{2(pc)}, \tag{5}$$

where e is the charge, E is the electric field, L is the field length (6 m), p is the momentum, and c is the light velocity. M_{K^-} and M_{BG} are the masses of K^- and an unwanted particle, respectively. The beam was focused vertically by means of the quadrupole doublet Q3-Q4 with the vertical magnification factor of about 0.88 at the position where the slit for the mass selection (mass-slit) was placed. A potential of 600 KV was applied across the positive and negative electrodes. The distance between the electrodes was 10 cm. It was filled with mixed gas of Ne-He (36%) with the pressure of about 3×10^{-4} torr in order to prevent electric discharge. The vertical separation between the K^- and the π^- at the mass-slit was about 4 mm. The gap of the mass-slit was typically 1.02 mm and its vertical position was optimized so that the maximum intensity of K^- was obtained. The typical K^-/π^- ratio of the beam was 1/4 with K^--intensity of 2×10^4/spill.

Finally, the beam was focused on the target by using a pair of quadrupole magnets (Q6 and Q7). The beam size at the target center was 7.8 mm (r.m.s) in horizontal and 5.8 mm (r.m.s) in vertical with the width of incident angle of 104 mrad (r.m.s) and 27 mrad (r.m.s) in horizontal and in vertical, respectively.

The momentum bite was 3.6 % (FWHM), and the beam had a momentum dispersion of about 2.4 MeV/c per mm at the target point as shown in Fig.5, which was obtained in the analysis of beam particles described below.

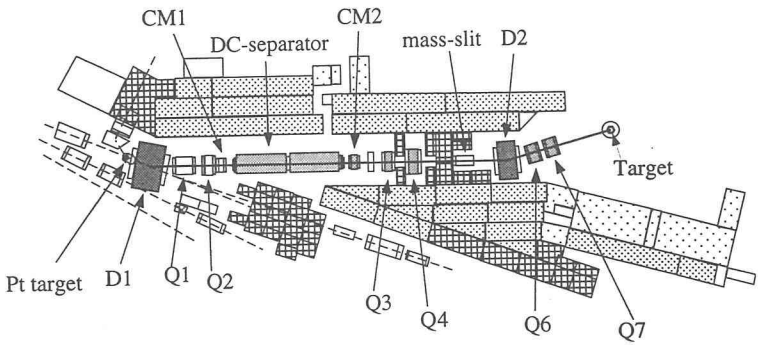

Fig. 4. Schematic view of the K2 beam line. Detector elements in the beam line are shown in Fig.2(a).

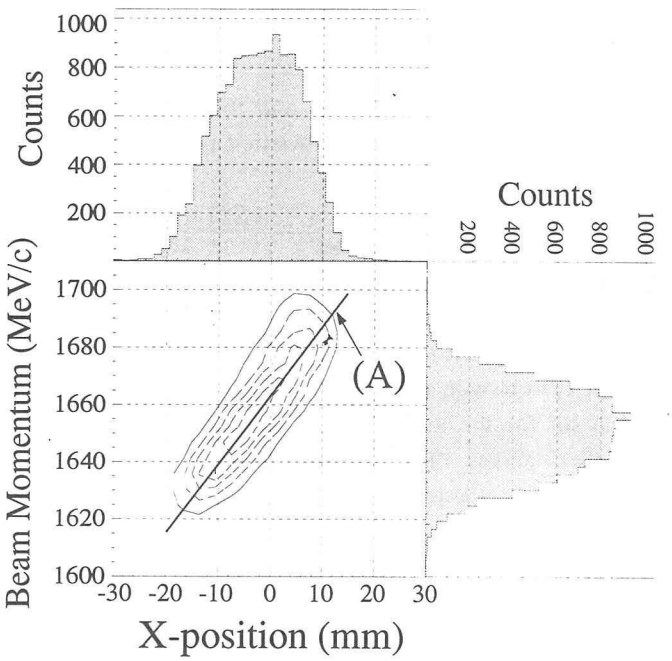

Fig. 5. The beam momentum dispersion at the target point. The correlation of the momentum p and the position x is parametrized as p(MeV/c) = 1664(MeV/c) + 2.4(MeV/c/mm) × X-position (mm), which is shown as line (A).

2.1.2 Measurement of the Incident Momentum using the Beam Line

The momentum measurement and the particle identification of the beam particles were performed by using the beam line as a spectrometer. As shown in Fig.2, the detector system in the beam line comprised five sets of tracking chambers (BPC1-5), two beam hodoscopes (T1,2) and a silica aerogel Čerenkov counter (BAC). Additionally, a veto counter was installed to reject events caused by a beam halo.

The K^- in the beam was tagged using BAC. The BAC contained a block of silica aerogel which was 8 cm wide, 8 cm high and 3 cm thick. It had a refractive index of 1.041 which corresponds to the β threshold of the Čerenkov radiation of 0.961 ($\beta_{K^-} = 0.959$ at 1.66 GeV/c). The Čerenkov light was detected with a photo-tube R1250 (Hamamatsu), which was sensitive to single photon. The fringing field of the spectrometer magnet (SP) was compensated by a compensation coil surrounding the photo-tube. The π^- was reduced to 0.8% of the K^-'s using BAC.

The contaminations of π^-'s and $\bar{p}$'s were reduced to 10^{-4} by means of offline analysis using the time-of-flight technique between the scintillation counters T1 and T2 which stood 6 m apart each other. The sizes of the scintillators (NE pilot-U) T1 and T2 were 5 mm thick, 5 cm wide, and 10 cm and 5 cm long, respectively. They were viewed by fast photo-tubes R2083 (Hamamatsu) from both ends. The time-of-flight resolution for the beam particles was 85 psec (r.m.s).

The momentum of each beam particle was determined using the beam-line magnets (see Fig.4) and the BPC's. The BPC's were multi-wire proportional chambers having anode wires being spaced every 1 mm located 4 mm from carbon cathode planes. The anode wires were made of gold-plated tungsten whose diameters were 10 μm. The BPC1,2 were located upstream of D2, and BPC3,4,5 were located downstream. The vertical position of the beam was measured with BPC1, BPC4 and BPC5, which had X and Y-planes, while other chambers had only X-planes. A "magic gas", which was a mixture of Ar, freon (CF_3Br), C_4H_{10} and methylal with the mixing ratio of 73:24:0.5:3, was used at the atmospheric pressure. The parameters and typical efficiencies of the BPC's are summarized in Table.1.

Table 1. Characteristics and performance of the beam chambers (BPC1-5)

BPC	1-X	1-Y	2-X	3-X	4-X	4-Y	5-X	5-Y
number of read wires	112	64	112	80	112	64	80	64
location from target center (mm)	6318	6302	5662	4693	2726	2710	615	631
typical efficiency (%)	93.9	81.4	93.9	91.4	93.4	94.0	96.2	77.3

2.2 K^+ Tagging Spectrometer

2.2.1 Spectrometer Magnet

The spectrometer magnet (SP) was a window-frame-type dipole. It had a 50-cm gap, 100-cm aperture and 80-cm long pole piece. It had end-guard plates of 8 cm thick located 80 cm from the center. The downstream end-guard had a 60-cm gap and 110-cm aperture, while the front end-guard had a 30-cm gap and 50-cm aperture. The front one was smaller than the other in order to minimize the fringing field at the target point, since the magnetic field made a distortion of images of tracks in the electrostatic-type IIT (see Sec.2.3).

The magnet center was located 130.0 cm from the target center along the beam axis. The SP was rotated from the beam direction by 0.15 radian in the horizontal plane, which was optimized to the scattered particle with momentum of 1.2 GeV/c.

The beam particles were bent by about 0.2 radian and went away from the sensitive area of the aerogel Čerenkov counter and that of the most downstream tracking chamber (DC3, see Sec.2.2.5).

The shape of the field is shown in Fig.6. The field mapping was done with the accuracy of 0.1 % which was achieved by careful measurements with the correction on Hall-planar effect [32].

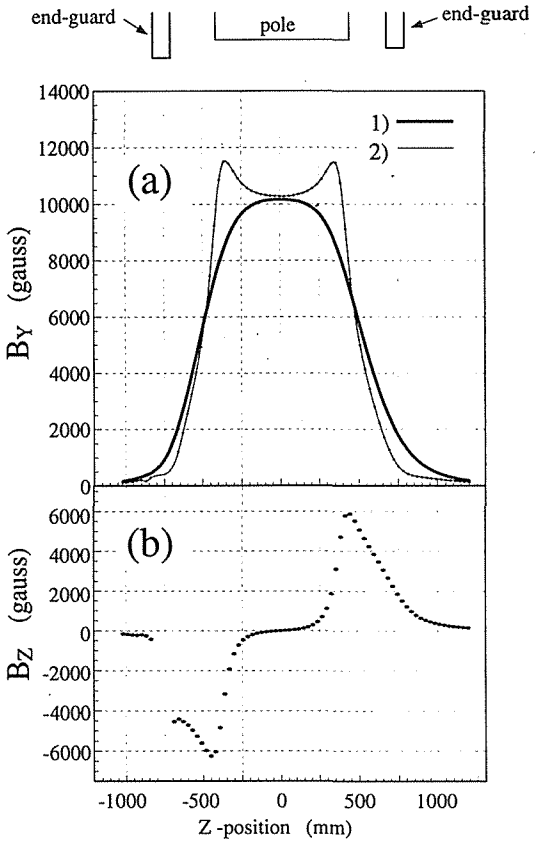

Fig. 6. Magnetic field of the spectrometer magnet SP. a) Field strength of Y-direction (vertical) along the beam direction (Z) at X = 0 (magnet center in horizontal) and 1) Y = 0 (center) 2)Y = -200 mm. b) Field strength of Z-direction at X = 0, Y = -200 as a function of Z-position.

2.2.2 Acceptance

The geometrical acceptance of the spectrometer system for scattered particles was defined by the hodoscope YH located just before the aerogel Čerenkov counter (SAC). The acceptance was 0.09 sr for the particle with momentum of 1.1 GeV/c. It was ± 0.21 radian in horizontal and ± 0.12 radian in vertical. Along the beam axis (0 degree), a counter BV vetoing non-interacting particles was located in front of SP in order to reduce fake-triggers due to decays of K^-'s in the beam. It vetoed the area of $\theta < 0.063$ radian in azimuthal. The acceptance is shown as a function of the

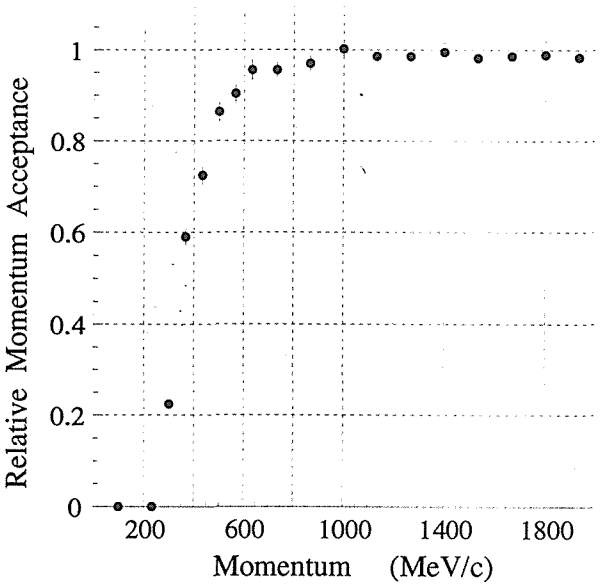

Fig. 7. Acceptance of the spectrometer as a function of the momentum of scattered particles. The acceptance is normalized to that for the particle of 1.0 GeV/c.

momentum of scattered particles in Fig.7. The acceptance was constant within 3% for the particles of the momentum higher than 0.9 GeV/c.

2.2.3 TOF Counters

To discriminate K^+'s from π^+'s and protons, the velocity of scattered particles was determined by the time-of-flight between T2 and a forward TOF hodoscope (FTOF) (see Fig.2), combining with the flight length measured with the tracking chambers. The schematic view of FTOF is shown in Fig.8. The FTOF consisted of 24 scintillators which were 12.0 cm wide and 3.0 cm thick. Ten of them in the central region were 130 cm long and the others were 110 cm long. They were installed vertically at the distance of 500 cm from the target along the central orbit of 1.2-GeV/c particles, being staggered with overlapping of 2.0 cm each other as shown in Fig.8. The scintillators were viewed by photo-tubes H1949 (Hamamatsu) from the top and the bottom.

For the TOF measurement we used 12-bit TDCs[2], which had a time resolution about 27.5 psec/count. All the TDC channels were calibrated with a TDC-calibrator within the accuracy of 0.1 psec/count. The linearity of the TDC was better than 1/2000. In order to reduce the difference of transmission velocities in the cables due to the variation of temperature, all the cables were arranged to keep in the same path. The timing drift was checked run by run (typically 4 hours) by adjusting at the reconstructed-mass peaks of π^+'s and protons. The fluctuation of timing due to the

[2] manufactured by REPIC Co.

[3] The Garfield simulates the field shape two-dimensionally. The program was originally coded by R.Veenhof for the application to the HELIOS experiment at CERN.

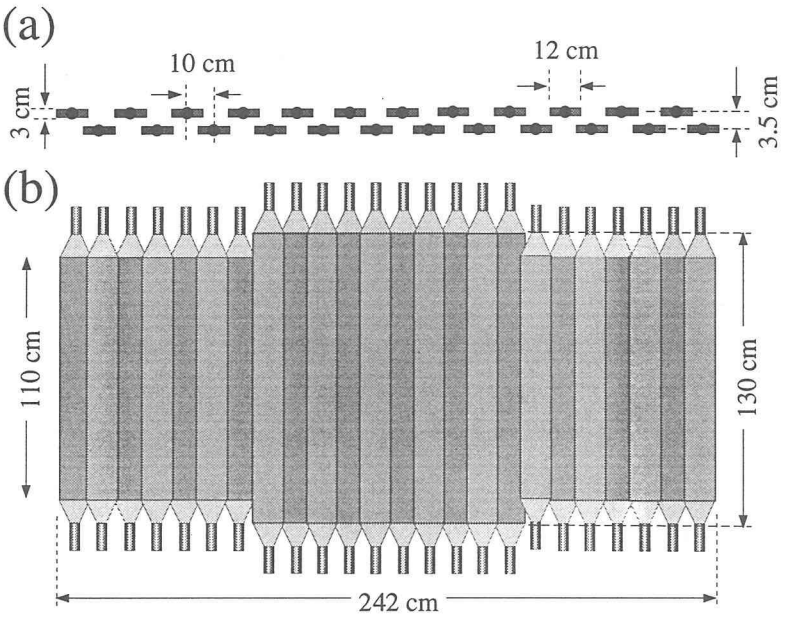

Fig. 8. Schematic view of the FTOF counters. (a) Top view. (b) Front view.

pulse-height difference in the discriminators was corrected with functions inversely proportional to the 1/4th power of the pulse-height. The average time resolution of the TOF measurement from T2 to FTOF was 110 psec (r.m.s).

The FTOF was also employed to measure vertical hit positions of particles on FTOF, which were given by the time difference of the two signals from the PMT's on the top and the bottom. The obtained position resolution was 14.8 mm (r.m.s).

2.2.4 Cylindrical Drift Chamber

In order to detect the decay products of the H with high momenta, as well as the incident K^-, scattered K^+ and other charged particles coming out of the target, a cylindrical drift chamber (CDC) was fabricated. The CDC consisted of eight layers, whose radii were 160 mm to 384 mm as shown in Table.2. The height of CDC was 90 cm. The third and the sixth layers had wires tilted by 5.71° to the vertical direction in order to obtain vertical information. There had been no wire in the space for installation of the horizontal read-out system of the SCIFI-target as shown in Fig.9. All the wires were placed between two stainless steel plates (end-plate)

Table 2. Configuration of CDC for each layer

Layer	1	2	3	4	5	6	7	8
radius of sense wire position (mm)	160.0	192.0	224.0	256.0	288.0	320.0	352.0	384.0
number of read wire	32	42	48	60	69	76	87	97
direction of wire	Y	Y	stereo	Y	Y	stereo	Y	Y
typical efficency (%)	93.0	93.0	93.3	91.5	94.8	94.1	96.0	90.5

supported by eight poles. The anode wires were made of gold-plated tungsten of 20 μm ϕ. The potential wires and the wires for field shaping were the gold-plated Cu-Be of 100 μm ϕ. These wires were positioned to the end-plates within the accuracy of 30 μm using "feed-throughs".

The chamber consisted of a number of fine segmented independent cells, whose configuration was similar to that of the "TASSO-chamber" [33]. All the cells had identical structures, with the drift space of 11.2 mm from the cathode wires to the anode wire as shown in Fig.10. The cell structure has been optimized using the field simulation code, Garfield[3].

We used a gas mixture of argon and ethane (1:1). The voltage supplied to the cathode wires was -2510 V. The corresponding maximum drift time was about 220 nsec. By tracing the tracks in the CDC back to the SCIFI-target, it was possible for the CDC to eliminate accidentally overlapped tracks in the SCIFI image.

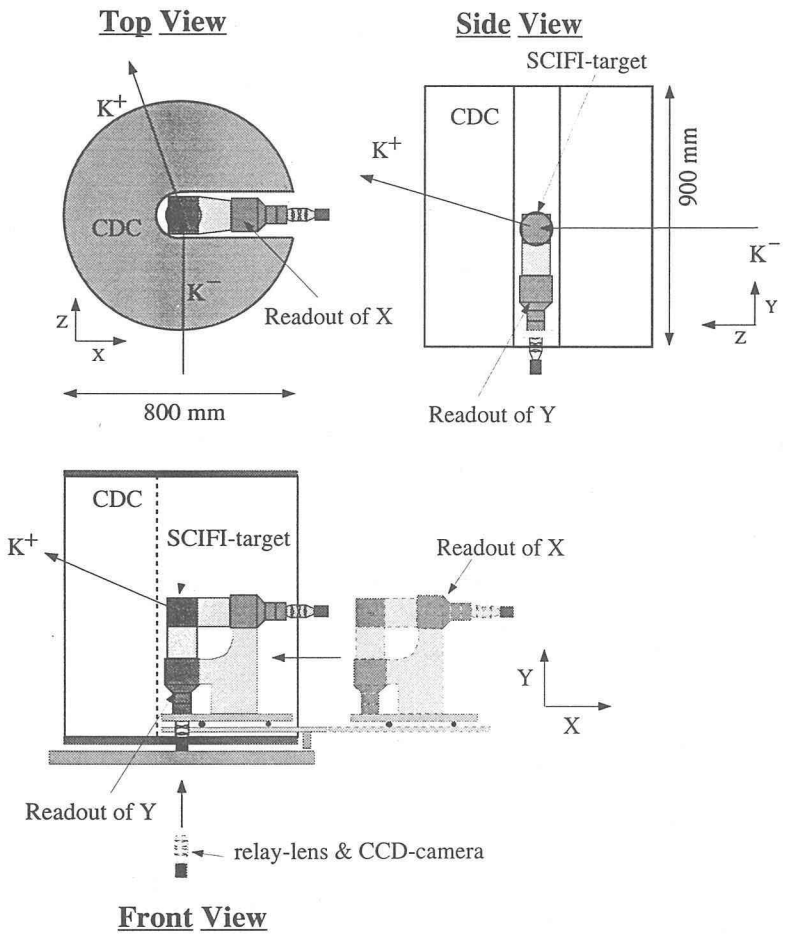

Fig. 9. Schematic view of the detectors around the target: the CDC and the SCIFI-IIT-CCD systems.

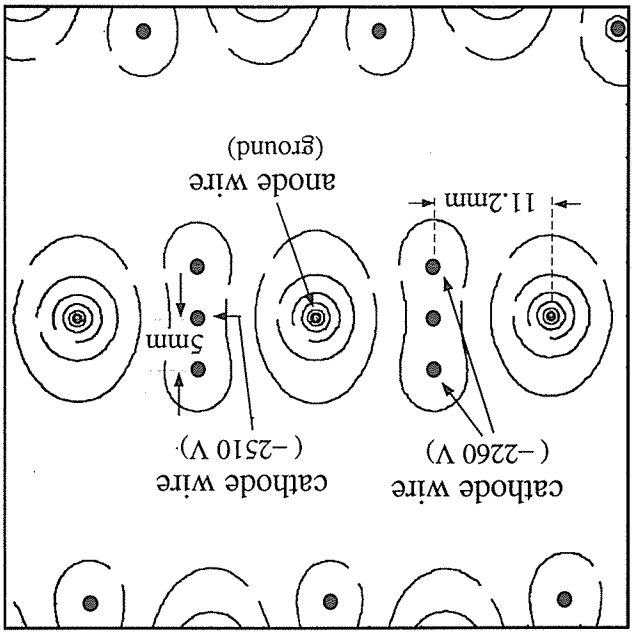

Fig. 10. Cell structure of the CDC. Contour plot represents the shape of the field simulated with Garfield (see text).

The TDC (TKO-Dr.T KEK) which we employed for digitization of the drift time had a time resolution of about 0.7 nsec per count. The overall position resolution of 270 μm was obtained for tracks of minimum-ionizing-particles.

2.2.5 Tracking Chambers

Tracks of scattered particles were measured using tracking chambers : the CDC (see Sec.2.2.4) and the drift chambers DC1, DC2, and DC3. The characteristics of the DC1,2, and 3 are summarized in Table.3.

The DC1 had a size of 500 mm in width and 350 mm in height. There were four anode planes to measure the X, X', Y and U coordinates. The X and X' planes were staggered by the drift space of 5 mm. In the U-plane, the sense wires were tilted by 15 degrees from the vertical direction. The cell structure of DC1 is shown in Fig.11(a). The cathode planes were made of 15-μm-thick Kapton foils with aluminum coating on both sides.

The effective area of DC2 was 1200 $\times$ 1200 mm^2 with four anode planes of X, X', Y and Y'. The sense wires were surrounded by hexagonally located potential wires as shown in Fig.11(b). The spacing of the sense wires was 9 mm. The DC2 was located just downstream the end-guard plate, covering the full aperture of the magnet. The DC1 and DC2 were designed to cope with the high-rate operation for the beam passage.

The DC3 had a sensitive area of 180 cm in horizontal direction and 90 cm in vertical. The location of DC3 was about 1.2 m downstream the DC2. The chamber had four planes, X, X', Y, Y'. The cell structure of each plane is seen in Fig.11 (c)

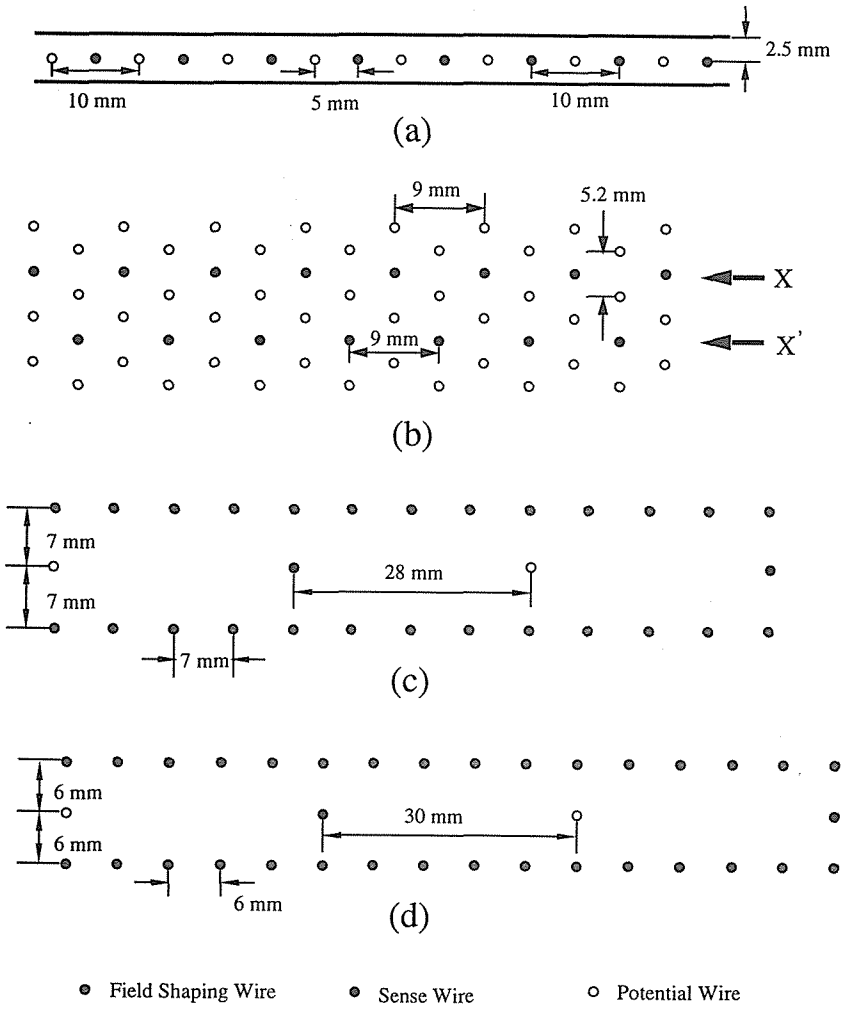

Fig. 11. Cell structures of a) DC1, b) DC2, c) DC3-XX' planes and d) DC3-YY' planes

and (d). The drift spaces were 28 mm for the X and the X'-planes and 30 mm for the Y and the Y'-planes.

The mixed gas of Ar-ethane (1:1) was used for all the drift chambers, DC1, 2, and 3. The drift time was digitized with TKO-TDCs by means of the same manner as in the case of the CDC. The typical efficiency and the position resolution of each chamber are shown in Table.3. The obtained resolution for the Y-plane of each chamber was relatively worse because of less redundancy for the vertical direction to fit the tracks, which limited the chamber calibration.

Table 3. Characteristics and performance of Drift Chambers (DC1-3)

chamber	DC1	DC2	DC3
plane	XX'YU	XX'YY'	XX'YY'
anode-wire spacing (mm)	10.0	9.0	X:56/Y:60
anode-wire diameter (μm)	20.0	20.0	20.0
anode-wire potential (V)	-	-	+ 1000
anode-wire material	Au-plated W	Au-plated W	Au-plated W
potential-wire H.V (V)	-1900(cathode plane)	-2100	-3000
potential-wire material	Au-plated Cu-Be	Al	Au-plated Cu-Be
potential-wire diameter	75 μm ϕ	200 μm ϕ	150 μm ϕ
number of read wire	XX':48/Y:32/U:40	XX':128/YY':96	XX':32/YY':16
location (Z position from target)	775mm	2305mm	3545mm
dimension X × Y(mm)	500 × 350	1200 × 1200	1800 × 900
typical efficiency (%)	99.5	90.3	93.5
position resolution (μm rms)	XX':220/Y:400/U:200	XX':230/YY':270	XX':310YY':390

2.2.6 Silica Aerogel Čerenkov Counter

One of the major backgrounds was π^+'s whose yield was two order of magnitude as large as that of K^+'s. In order to reduce the detection rate of π^+'s, a Čerenkov counter SAC was installed. We used silica aerogel (manufactured by Gadelius Co.) which had a refractive index of 1.041 (β_{th}=0.961, density ρ =0.20 g/cc) to distinguish K^+'s from π^+'s in the momentum range of 0.5 GeV/c to 1.5 GeV/c.

The effective size of SAC was 200 cm and 100 cm in horizontal and vertical directions, respectively. The walls of the diffusion box were covered with highly reflective white sheets (Millipore). It was equipped with 38 photo-tubes (Hamamatsu R1250 and RCA 8854) on the top and the bottom. In order to minimize the knock-on electrons, the entrance windows on the both surfaces were made of 100 μm Mylar sheet coated with aluminum (12 μm). Three pieces of the aerogel which had dimensions of 25 × 25 × $3cm^3$ were stacked. N_2 gas flowed to prevent the deterioration of the aerogel due to the moisture during the run.

The SAC was located downstream of DC3 in order to avoid the multiple scattering before DC3. The location was also helpful to minimize over-killing of (K^- ,K^+) reaction events which associated with relatively high-momentum π's from the H decay or the hyperon decay. These π's are swept out by the magnet SP.

The average number of photo-electrons for 1.6-GeV/c π^+ was about 3. The obtained efficiency as a function of β and the survival rate (inefficiency of SAC) as a function of the corresponding K^+ momentum are shown in Fig.12 (a) and (b), respectively. The survival rate of K^+'s in the momentum region below 1.6 GeV/c was 85 %. It was due to the fake hit of SAC. The fake hit was mainly caused by the accidental coincidence of thermal noises of the PMTs. The fake hit rate due to the knock-on electron was calculated to be 1.3 % at 1.6-GeV/c K^+, which was negligibly small compared to the accidental coincidence rate. The efficiency of SAC was monitored during the run using data obtained without veto of π^+'s by SAC in the trigger. It was also checked with the 1.6-GeV/c K^+ beam, whose β is 0.956.

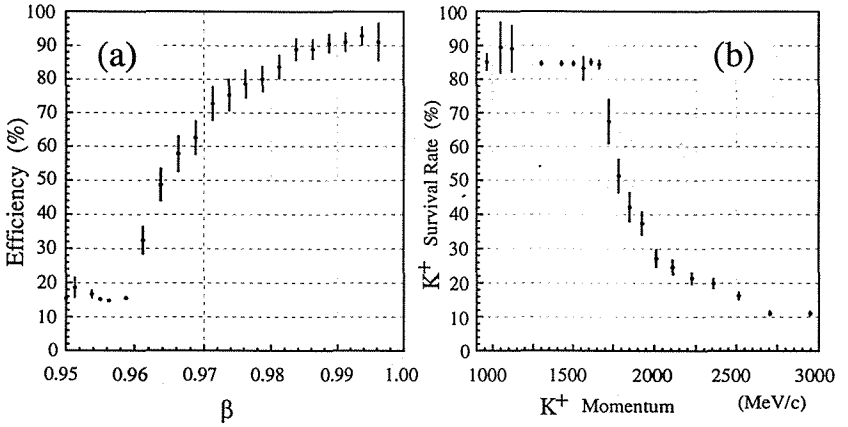

Fig. 12. (a) The veto efficency of SAC as a function of β . (b) The K^+ survival rate from veto with SAC as a function of K^+ momentum.

2.2.7 Charge Hodoscope

In order to eliminate negative charged particles, a hodoscope CH was installed 45 cm downstream of the target center (in front of the forward end-guard plate). It was used for the first-level online trigger as well as the second-level trigger (see Sec.2.4). The CH consisted of 12 scintillators each of which was 3.5 cm wide, 17 cm height and 1.0 mm thick.

2.3 Scintillating Fiber Active Target System

A scintillating fiber target (SCIFI-target) [25, 26] was used as a vertex detector. The tracks of the charged particles in the vicinities of the reaction vertices were detected in this target which had a volume of about 1 liter. It was designed to provide three-dimensional information on the tracks and to be triggerable with a time resolution of several μsec to avoid the overlap of the tracks of more than one events.

The SCIFI-target system consisted of a block made of scintillating fibers and its readout system [25, 26]. The schematic view of the system is shown in Fig.13. Each of the X and Y projections was read out through a set of image-intensifier-tubes (IIT), an optical relay-lens and a CCD-camera.

2.3.1 SCIFI-Target

The SCIFI-target consists of about 30,000 plastic scintillating fibers, SF81 (KURARAY), of 20 cm long. The cross section of the scintillating fiber had a square shape with the dimension of 500 μm $\times$ 500 μm which had a core of 480 μm $\times$ 480 μm coated with cladding material of 10 μm in thickness. The core was made from polystyrene $(CH)_n$ with the density of 1.06 g/cm^3. The refractive index of the core was 1.59. The cladding was made from PMMA, $C_5H_8O_2$, whose index was 1.49. The density of PMMA was 1.18 g/cm^3. The wave length for the peak output light was 437 nm (blue). The specifications of the SF81 are summarized in Table.4.

Fiber sheets of 500 μm thick, 20 cm long and 8 cm wide were stacked in the X (horizontal) and the Y (vertical) directions alternately as shown in Fig.3, providing the

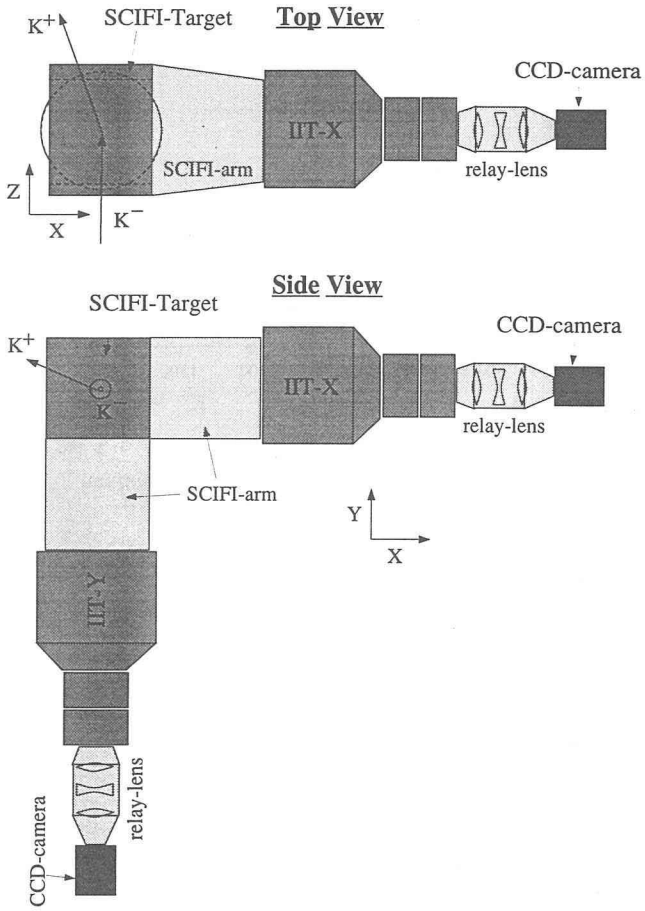

Fig. 13. Schematic view of the SCIFI-IIT-CCD system.

Table 4. Specifications of the scintillating fiber, SF81.

core material	polystyrene $((CH)_n$ 480 μm $\times$ 480 μm)
core density	1.06 g/cm^3
core index	1.59
wave length	437 mm
cladding material	PMMA ($C_5H_8O_2$)
cladding thickness	10 μ m
cladding density	1.18 g/cm^3
cladding index	1.49

total effective volume of $8\times8\times10$ cm^3. The number of fiber sheets stacked was 92 for each direction. The sheets were glued with a sort of black PMMA. The average thickness of the glue was 50 μ m. The spaces between the fiber sheets for both projections were reduced from 550 μm to 350 μm in the fiber-arms in order to make the fiducial size viewed by the IITs (80 mm ϕ) larger. The dimensions of the SCIFI-

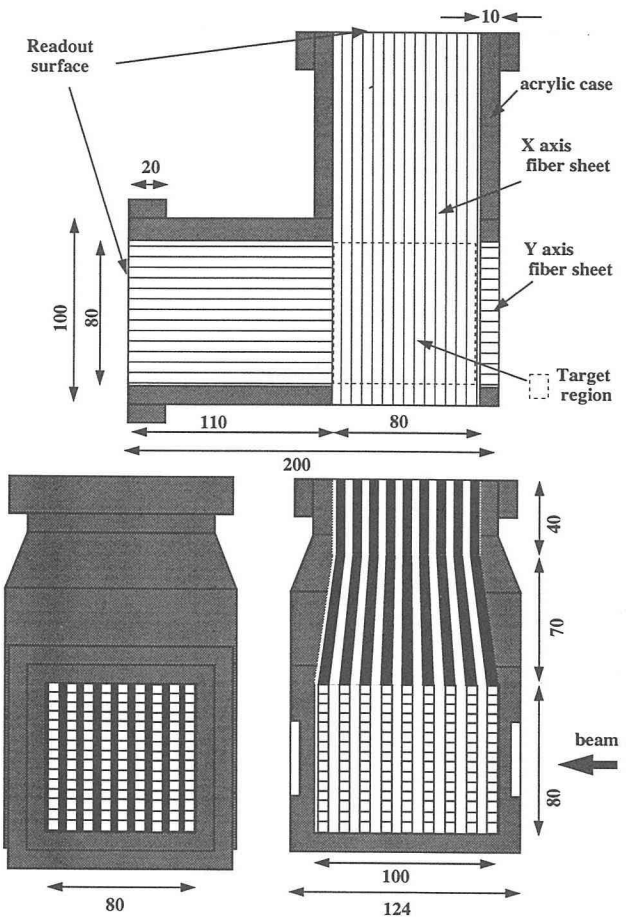

Fig. 14. The dimensions of the SCIFI-target. All the units in the figures are in mm. The fiber size is shown 10 times as large as the real size.

target are shown in Fig.14.

2.3.2 Image Intensifier Tube

The output lights from the fiber target were amplified with the IIT. The type of the IIT was PP0040 which was manufactured by Delft Corporation. The schematic view of the IIT is shown in Fig.15. The IIT had a cascade structure of three individual image intensifiers. The first stage was of "converter type" with a large effective entrance area of the diameter of 80 mm, which was labeled as PP0040c. The second stage and the third stage were of the same type (XX1450) which had micro-channel-plates (MCP) to amplify the image. The second stage and the third stage were operated in a gating mode with a trigger pulse using information from the counter system.

Each stage of the IIT had phosphor on the anode as an electron-photon converter. Phosphor was employed also for optical delay, since phosphor held the image in the duration of its optical decay time.

The SCIFI-target was attached to the entrance window of the first stage with optical grease. The entrance window consisted of optical fibers. The first stage was operated in DC mode with the supplied voltage of 20 KV. The size of the image was reduced with the electrostatic focusing field by the magnification factor of 0.19 at the center and 0.2 at the edge[4] (r=40 mm), which provided an image on the second stage. The photon amplification factor was about 8. The rate to obtain available pictures was limited by the decay constant of the phosphor on the first stage because the picture of only one event could be obtained during the decay time of the phosphor without overlapping of tracks. Thus, it was preferable that phosphor of the first stage had a short optical decay constant. The phosphor for the first stage was P-24 (ZnO,Zn), whose phosphorescence has a peak wave-length of 510 nm with the decay constant of 2.4 μsec.

The second and the third stages of the IIT had an optical fiber-windows of 18 mm ϕ. The gain of the photon in each MCP was about 3×10^3 with the supplied voltage of 750 V. They were operated with the triggerable gate voltage between the photo-cathode and the MCP besides the bias voltage. The applied gate-voltages were -200 V to open the gate and +50 V to close as summarized in Table.5.

Table 5. High voltage gate supplied to the second and third stages of the IIT.

	second gate	third gate
typical repetition rate	55 Hz	8 Hz
gate Width	2.5 μsec	1.0 msec
trigger	first-level trigger	second-level (Mass-Trigger)
decision time	300 ns	15 μsec
delay at internal circuit	$\leq$ 100 ns	$\leq$ 100 ns

The second stage was gated by the first-level trigger pulses (see Sec.2.4.1), which were made of the fast signals from the Čerenkov counters and scintillator hodoscopes, within 400 nsec after a reaction occurred in the SCIFI-target. The gate width was 2.5 μsec which determined the time resolution of the picture for reactions. The image amplified by the MCP was stored in the phosphor P-20, which had a decay constant of 50 μsec. The second-level trigger pulse (see Sec.2.4.2), gated the third stage of the IIT within 15 μsec. The applied gate width was 1 msec.

The intrinsic position resolution of the IIT was about 25 μm on the surface of the entrance-window of the first stage. The image of one photon had a size of about 180 μm (r.m.s), which was mainly due to the diffusion of image in the phosphor of the first stage. The number of background spots in the pictures due to the thermal noise of the IIT system was negligible in the gated operation.

[4] The difference of the demagnification factor is called the pin-hall distortion, which was corrected in the offline analysis

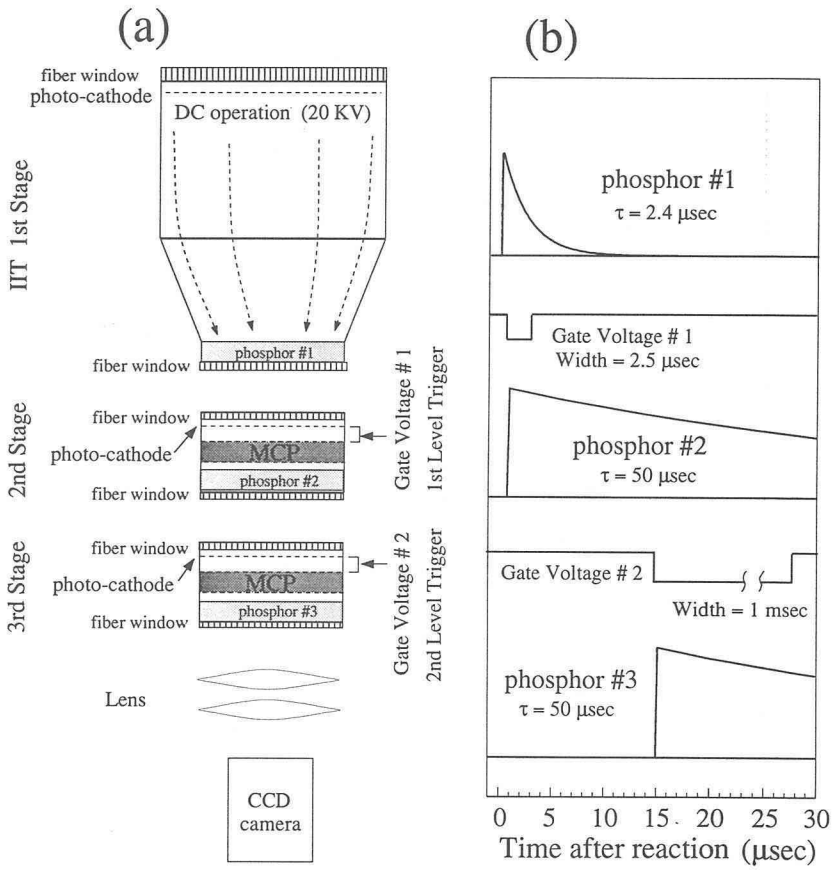

Fig. 15. (a) The schematic view of the IIT. (b) The timing chart of the gate operation of the IIT.

2.3.3 CCD Camera

The gated image amplified by the IIT was viewed by the CCD camera through the optical lens (relayed lens). The size of the image was reduced to by 1/13 to match the size of the CCD-chip in the CCD camera from the first stage of the IIT to the relayed lens. We used a CCD camera, SONY XC-77, which had 768 × 493 pixels with the size of 11.0 μ m × 13.0 μ m. It means that the size of the single fiber corresponded to about four pixels in the CCD camera. The signal from the CCD was serially read out with the cycle of 30 Hz of usual NTSC format.

2.3.4 Image Digitizer

The digitization of the X and Y images from the CCD camera was performed by four special modules, Clock Coordinate Generator (CCG), Flash ADC (FADC) and FI/FO buffer module equipped with first-in/first-out memories (FI/FO) for each projection. The read-outs of two CCD cameras were synchronized by an external common clock from the CCG module as shown in Fig.16. When the second-level trigger fired, the CCG module started the sequence of the digitization. The timing of

the external clock was not synchronized with the trigger. It resulted in some overhead time of 15 msec at the maximum to start the transfer.

The FADC was synchronized with the video signal by the same external clock. The digitized signals smaller than a preset threshold value were rejected to reduce the data size. The digitized data for pixels were stored in the FI/FO module. Typical data size of an event was 2 K long-word for each projection. The data in the FI/FO module was taken by a data acquisition system operated by VME (see Sec.2.5).

Figure 17 shows a picture of typical event of the Ξ^- production. The sequential decay of $\Xi^- \rightarrow \pi^- \Lambda$ followed by $\Lambda \rightarrow \pi^- p$ is clearly seen. The quality of the data of the SCIFI-target, calibration methods and performances are described in the next chapter.

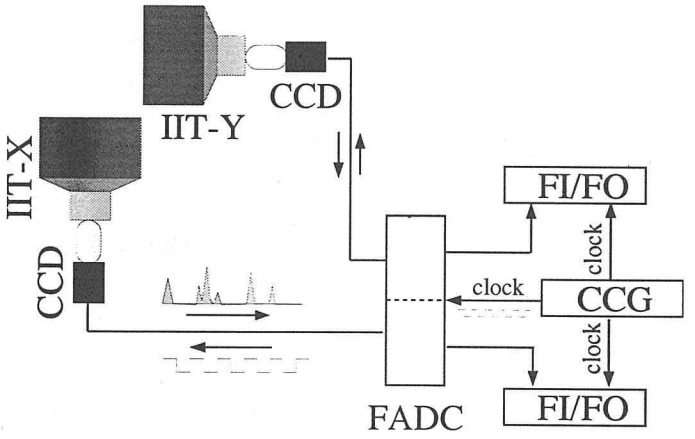

Fig. 16. The scheme of the operation of the CCD camera and synchronization of IIT-CCD system for the X and Y projections.

2.4 Trigger

2.4.1 First-Level Trigger

Main background for scattered K^+'s were π^+'s, protons and elastically scattered K^-'s. The rates of these particles were of the order of 10^3/spill, while the event rate of the (K^-, K^+) reactions of interest is of the order of 0.1 event/spill. The first-level trigger was designed to eliminate negative particles and fast π^+'s using the fast signals from the Čerenkov counters and scintillation counters.

The logic for the first-level trigger is as follows. We define the K^- beam signal as :

$$K_{BEAM} = SPILL \otimes \overline{BUSY} \otimes T1 \otimes T2 \otimes \overline{HV} \otimes \overline{BAC}, \tag{6}$$

where $\otimes$ represents the "AND" logic. The $SPILL$ is the spill-gate signal from the accelerator, $\overline{BUSY}$ represents a live-time signal from the online-data taking system. The $T1 \otimes T2$ is the coincidence signal of the TOF counters for the beam, and the HV is the signal from the beam-halo veto counter. The $\overline{BAC}$ represents the veto signal

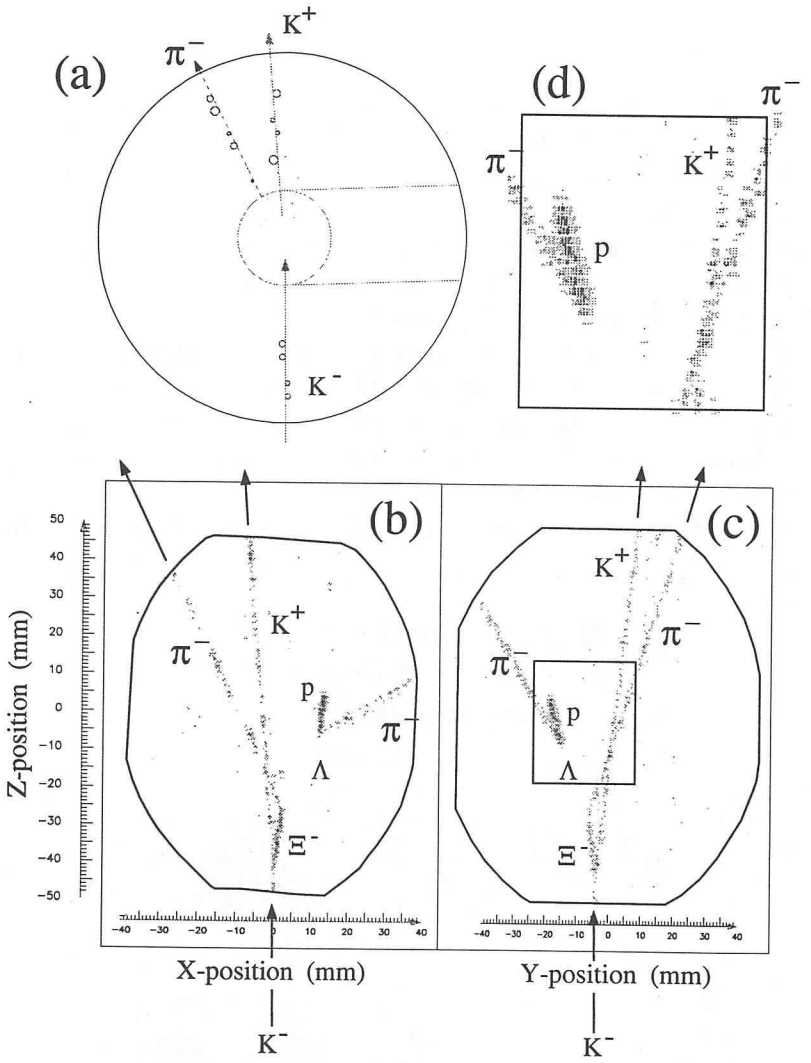

Fig. 17. A display of a typical Ξ^- production event: a) The K^- and K^+ were detected with CDC and were traced back into the SCIFI-target. b) The X projection of the image data of the SCIFI-target. The Ξ^-, which was produced at the (K^-,K^+)reaction vertex, decayed into $\Lambda\ \pi^-$. The π^- was detected in CDC. The Λ which decayed into π^- and proton is shown as clear V-topology. All these tracks are clearly identified also in the Y projection as shown in c). Combining these two projections, the tracks were reconstructed to a three-dimensional view. The size of the fiducial area is also shown. The detail of the central of the Figure c) is shown in d).

from the BAC, which rejected π^-'s in the beam.

The first-level trigger was formed as :

$$K_{BEAM} \otimes \overline{BV} \otimes YH \otimes \overline{SAC} \otimes (charge - trigger), \tag{7}$$

where BV represents the hit on the beam-veto counter. The requirements of $\overline{BV}$ killed the K^-'s which did not interact in the target or were scattered to a small angle. The hit on YH hodoscope is denoted as YH, which was required to eliminate fake-triggers due to neutral particles. The SAC represents the "OR"ed signal from all the photo-tubes of the Čerenkov counter SAC, which reduced π^+'s down to about 10%. The (*charge - trigger*) represents a logic which selects positive charged particles (charge trigger) using a matrix coincidence between the hit positions on FTOF and those on CH. The performance of the charge trigger is shown in Fig.18. Negative charged particles were reduced to 10^{-3} by means of this trigger. The efficiency of the charge trigger for positive charged particles was 95 to 99 % in the momentum range from 400 to 1700 MeV/c as shown in Fig.19 which was obtained using data collected without the charge-trigger in the first-level trigger.

The trigger rate at the first level was typically 55 Hz with the K^- intensity of 2 ×

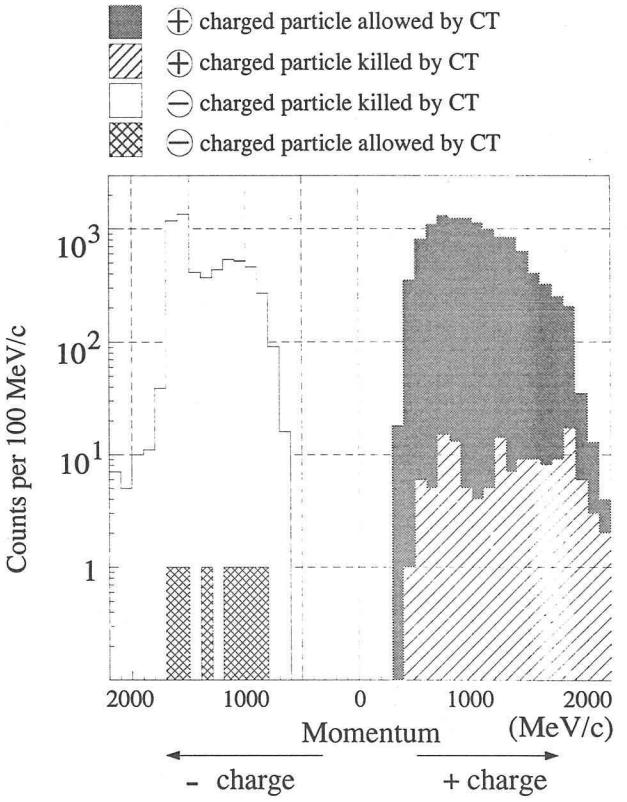

Fig. 18. The performance of the charge trigger in the events with single-CH hit and single-FTOF hit.

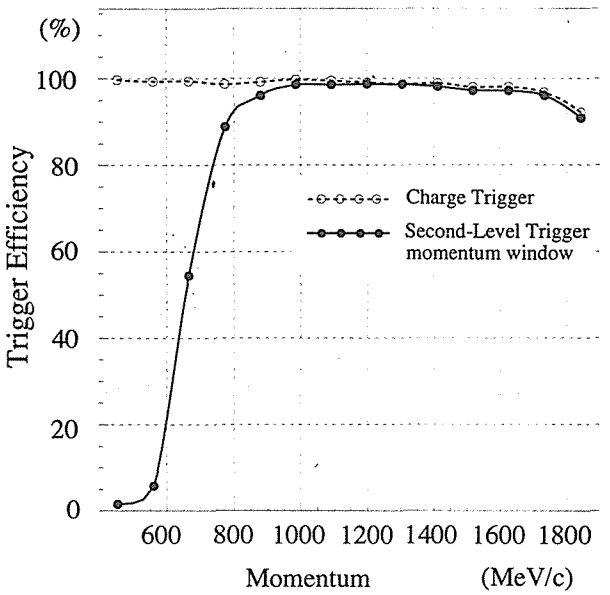

Fig. 19. Efficiencies of the triggers as a function of momentum of scattered particles. The dotted line is the efficiency of the charge-trigger. The solid line shows the momentum window of the second-level trigger (see the text).

10^4/spill. In addition, the second-level trigger, "mass-trigger", was developed in order to enrich (K^-,K^+) events for the CCD read-out of the SCIFI-target.

2.4.2 Second-Level Trigger

After the first-level trigger was applied, the major background was protons from (K^-,p) reactions in a momentum range from 0.5 GeV/c to 2 GeV/c. We selected K^+'s using the digitized data of the TOF and the momentum information obtained from the hit positions on CH and FTOF. The trigger was designed to calculate the mass of the scattered particles within 15 μ sec, whereas the holding time of the image in the phosphor at the second stage of the IIT was about 50 μsec.

The trigger scheme is shown in Fig.20. The combination of the hit counter numbers (ID #) of CH and of FTOF corresponded to the bending angles of the scattered particles by SP. The TOF information was obtained from the time difference between FTOF and T2. We used the fast enconding TDC system consisting of a TAC (Lecroy-TFC) and an ADC (Lecroy FERA-4403B). The TDC has a time resolution of 45 psec and its conversion time was 11.2 μsec. The ID # of FTOF and the time information were stored in the memory in the FERA module. The ID # of CH was stored in the FI/FO module (Lecroy Data-Stack).

The trigger sequence started just after the completion of the conversion of the TOF in the FERA module. The ID # of FTOF was encoded to 5 bits through the PLU module (Lecroy Programable-Logic-Unit). For each ID # of FTOF, the Data-Stack was cyclically scanned to make a combination with the ID # of CH (4 bit data). The combination was encoded to the 7-bit "MOMENTUM" data according to a table

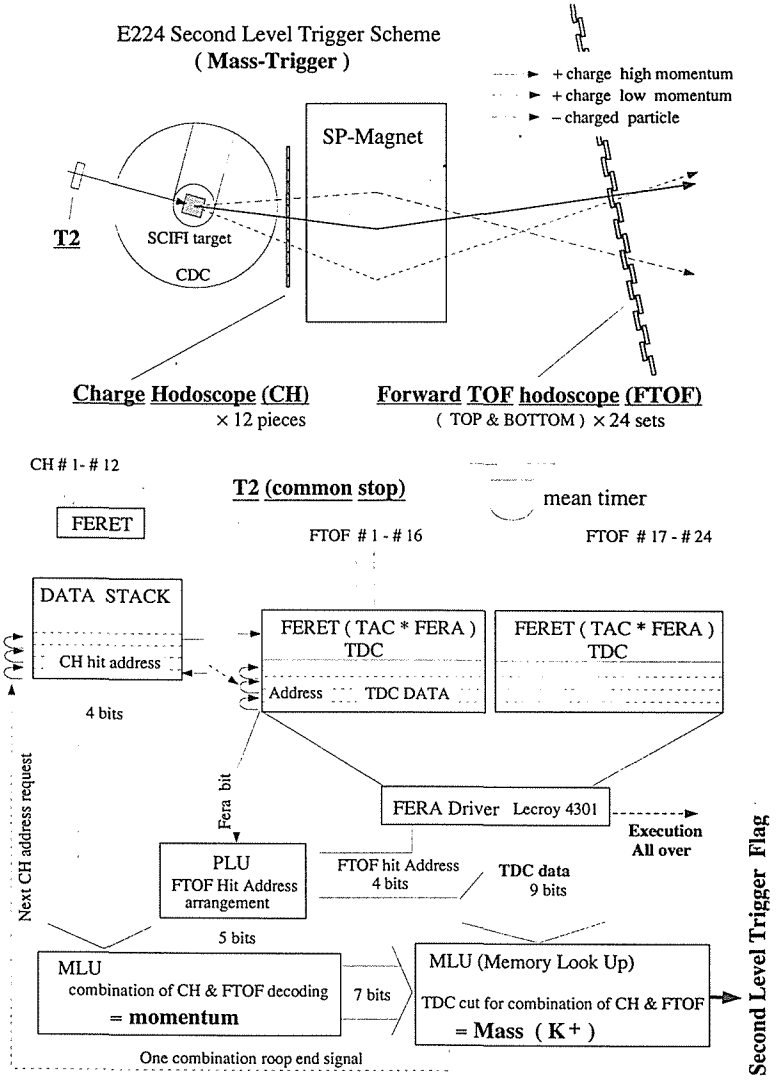

Fig. 20. Scheme of the second-level trigger

pre-loaded in a MLU (Lecroy Memory-Look-UP unit). At this stage, low-momentum particles were rejected, and particles in the momentum range of interest were enriched as shown in Fig.19. The 7-bit "MOMENTUM" was finally compared with the lowest 9-bit of the TDC data using another MLU module which contained 2^{16} bits of trigger-flag data according to the correlation between the TOF and "MEMENTUM" for kaons. The sequence continued until all the combinations of the hit counters of CH and FTOF were scanned. It took about 100 nsec to investigate one combination of CH and FTOF, and the trigger-flag was generated 14 μsec after the reaction occurred in the SCIFI-target.

The performance of the second-level trigger is shown in Fig.21. Protons were

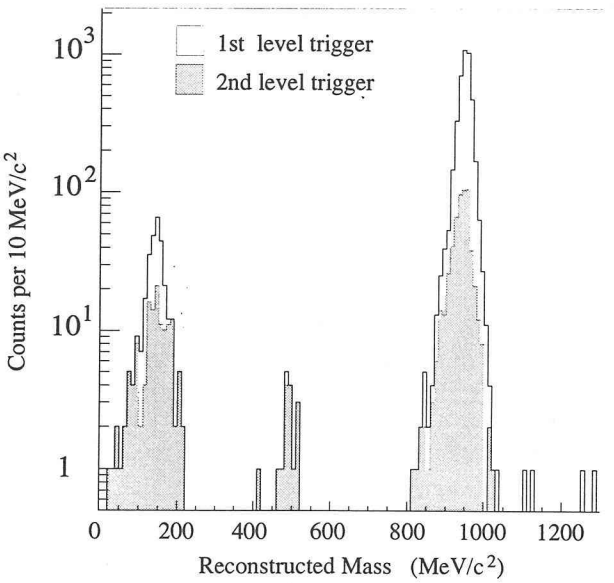

Fig. 21. The reconstructed mass distibutions of events which were obtained with the first-level and the second-level trigger. The performance of the second-level trigger which enriches K^+'s is shown. A single hit on CH is required for this graph.

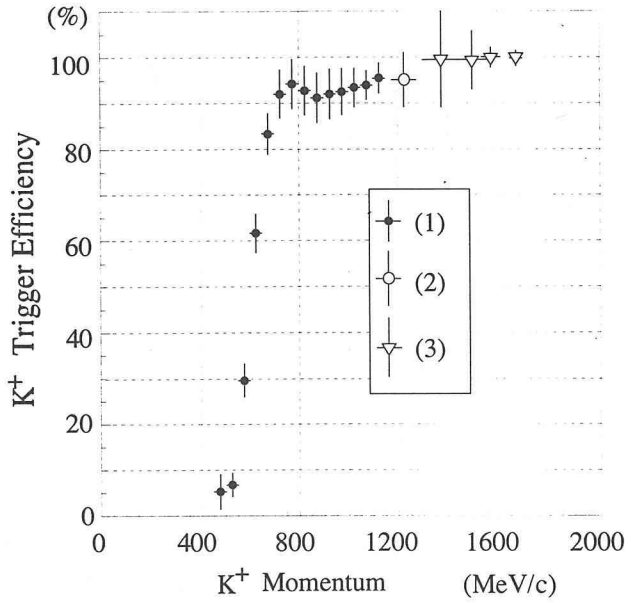

Fig. 22. Efficiencies of the second-level trigger (mass-trigger). Error bars are statistical ones. The efficiency was obtained with (1) (K^-,K^+) events in the momentum range from 300 to 1200 MeV/c. (2) (π^-,K^-) events and (3) events of elastic scattering of K^+ in higher momentum region.

reduced by the factor of 10. The efficiency of the second-level trigger for events taken with the first-level trigger is shown in Fig.22. The efficiency was larger than 90 % in the momentum range above 700 MeV/c. This triggering scheme enabled us to collect the image data with the dead time of about 20 %, which resulted in getting data with four times more statistics than in the case only with the first-level trigger.

2.5 Online Data Acquisition

The online data taking system consisted of three independent sub-systems. One of them was operated using a μ-VAX for the detectors in the spectrometer, and the other two were performed with VMEs for the X and Y-projections of the SCIFI-image readout system. Each sub-system had a 8-mm tape device. These sub-systems were synchronized with the trigger logics. The data were labeled with the same "event-tags" which were serial numbers of the events. All the data from the detectors in the spectrometer were taken when the first-level trigger fired in order to monitor the performance of the second-level trigger. The SCIFI image-data were taken only when the gate was opened with the second-level trigger.

All the data from the spectrometer were digitized by CAMAC and TKO modules [41]. The data of each event were transferred to the memory modules in the main crate with typical dead time of 3 msec. These data in the memory modules of the main crate were collected by the μ-VAX during beam-off periods through a crate-controller K3922 (Kinetic).

To monitor the condition of the second-level trigger, the data stored in the modules such as FERA and Data-Stack were taken directly with the μ-VAX about 1/4 of the whole runs. The procedure made the dead time longer by about 15 %.

The encoded data of the images of the tracks in the SCIFI-target which were stored in the FI/FO module were read out with a VME computer through a standard parallel I/O module. The dead time was typically 30 msec including operation time of the CCD cameras. The details of the data acquisition for the SCIFI-image are described in Ref. [34].

3 Data Analysis

Our purpose is to search for the H through the direct production in (K^-,K^+) reactions. Signature of H produced in this process is detection of a K^+ with higher momentum than that of quasi-free Ξ^- production process.

The analysis was started from the identification of the (K^-,K^+) reactions by means of the analysis of the spectrometer data. The obtained (K^-,K^+) reactions were examined using the data of the SCIFI-target to reject the background due to secondary interactions in the target.

3.1 Selection of (K^-,K^+) Events with Spectrometer

We collected the data of 3.1×10^7 events with the first-level trigger and 5.1×10^6 events with the second-level trigger in 4×10^5 spills during the run. The identification of (K^-,K^+) reactions is composed of two measurements, 1) analysis of

the beam particles and 2) identification of K^+'s by means of mass reconstruction.

3.1.1 Analysis of Beam Particles

Identification of K^- is indispensable for H search. We used separated K^- beam of 1.66 GeV/c in which the fraction of K^-'s was about 20 %. After the selection of K^- using the Čerenkov counter at the stage of the online trigger, there still remained contamination of particles such as π^-'s and $\bar{p}$'s in the beam. The π^-'s from K^--decay in flight had to be also eliminated. The background level in the acquired data was of the order of 10^{-2} to the K^-'s. These particles in the beam were rejected by mean of the measurement of TOF from T1 to T2, and tracking of particle trajectories using the data of the BPC's.

We applied cuts on the pulse heights of T1 and T2 to eliminate multi-particle hits on these counters, and we required hits on 4 X-planes of the BPC's out of 5. Tracking and momentum measurement were performed using the transport matrices of the beam line components which were obtained with the transportation program TURTLE with corrections of matrix parameters using the measured momentum of the beam with the K^+ spectrometer. The real tracks were selected by applying a cut on χ^2 of the fit. With the requirements above, the number of beam particles were reduced by 17.0%. The K^-'s which decayed after passing through T2 were rejected by comparing the tracks predicted by the BPC's with tracks found in the SCIFI-target. This background rejection is described later. The obtained momentum resolution $\frac{\Delta p}{p}$ was 5×10^{-3} (r.m.s).

The obtained TOF spectrum is shown in Fig.23. We used the K^-'s in the TOF

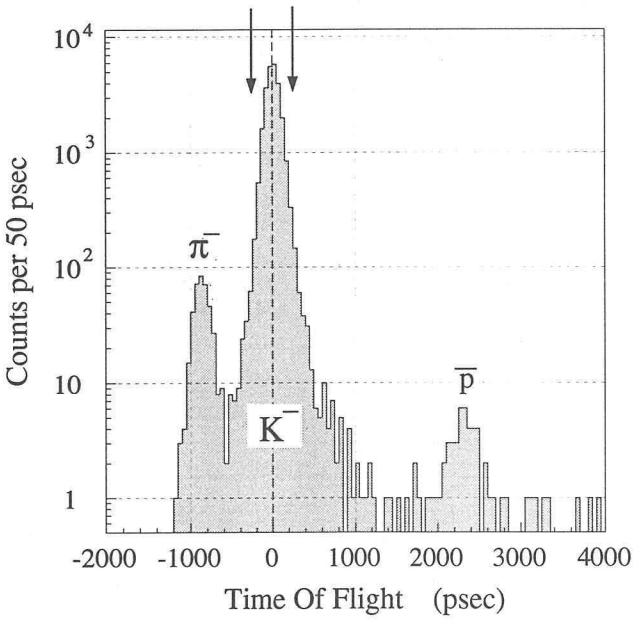

Fig. 23. The time-of-flight spectrum of the beam particles. The arrows represent the gate for the TOF spectrum to select K^-'S.

range of -250 to +250 psec in Fig.23. It covered the region of $\pm 3\,\sigma$ of the TOF resolution. With the selection procedures mentioned above, the number of the beam particles was reduced by 21.1 % from the total acquired data. The fraction of the remaining background was less than 10^{-4} which was evaluated with the TOF spectrum.

3.1.2 Track Reconstruction of Scattered Particles

The tracks in the spectrometer were reconstructed, and data summary tapes (DST) were made for the reconstructed data of (K^-, K^+) reactions. In order to save the computing time, the data were reduced through several stages of analysis procedures for making the DST. Those were 1) the pre-selection by the off-line "mass trigger" using the chamber information instead of the charge hodoscope (CH) (see Sec.2.4.2), 2) preliminary track finding with use of the correlation of the chamber hits, 3) track reconstruction with the spline method, 4) K^+ selection, and 5) track reconstruction with the Runge-Kutta method.

Pre-selection

At this stage the data reduction was performed by examining the correlation among the positions of hit wires in the chambers, the positions of the hit counters in FTOF and the TOF data. The scheme is similar to that of the second-level trigger. The planes of X and X' in DC1 and DC2 were used for the pre-selection. The momentum and the flight length were determined as a combination of the ID # 's of the hit counters in FTOF. Combining with the TOF data, the scattered particles were identified as demonstrated in Fig.24. For any combinations of the hits on FTOF and the hits on the chambers, the flight-path length and momentum of the scattered particle were obtained assuming the target position. The value of the TOF has a clear correlation with the hit-wire position as shown in Fig.24. By selecting the regions as seen in the figure, the K^+ candidates were enriched. Special care was taken not to eliminate the K^+'s in the momentum range less than 1800 MeV/c where the H dibaryon through the direct process was searched for. We required this selection both for DC1 and for DC2, and either for X or X' plane in each chamber in order to keep the efficiency to be larger than 95 %. Through this pre-selection, the data size was deduced by a factor of 25.

Preliminary Track Finding

The track candidates were searched for both upstream and downstream of the spectrometer magnet (SP) separately using a simple straight-line fit in the horizontal plane (X-Z).

In the region upstream of SP, at least four hits were required on six X-planes of CDC. The hits both on the X and X' planes of DC1 were also required. The displacement less than 10 mm was required between the horizontal hit position on DC1 and the projection of a track in CDC. The track candidates in the region downstream of SP were searched for using DC2, DC3 and FTOF. At least three hits were required for the four X and X' planes of DC2 and DC3. The straight-line fit was applied on those hits and the obtained track position was required to match with the hit counter of FTOF within 140 mm from the center of the counter. All the combinations of the upstream tracks and the downstream tracks were examined to find

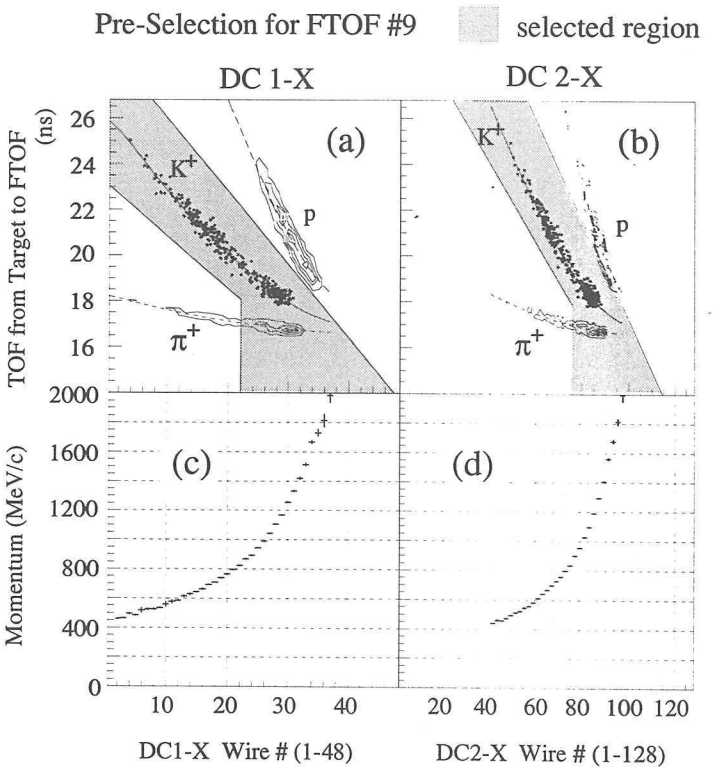

Fig. 24. Scheme of the pre-selection for the 9th counter of FTOF with DC1-X (a) and DC2-X (b). The hatched areas represent the selected regions. The momenta determined by the positions of the hit wires in (c) DC-1X and in (d) DC2-X are also shown. All the K^+'s in the final sample are overwritten as the dots to enhance the statistics.

a crossing point of the tracks. The crossing position in the X-Z plane was required to be in a region close to the center of the magnet.

For the vertical direction, at least three hits were required on the four Y or Y' planes of DC2 and DC3. The vertical positions of the track candidates downstream of the magnet should be within 12 cm from the ones obtained with the timing information of FTOF. Matching between the position extrapolated from the tracks downstream of the magnet and the hit position on the Y-plane of DC1 was also required.

Track Reconstruction by Spline Fitting Method and K^+ Selection

After the track finding procedures described above the track reconstruction was performed by means of quintic-spline fitting [42]. We introduced dummy planes every 10 cm from the target to DC3 for the spline-fit procedure [42]. The reconstructed tracks with a reduced χ^2 less than 10 were selected as good track candidates.

The track reconstruction efficiency of the spline fit in addition to the preliminary track-finding procedure is shown in Fig.25. It was about 80 % with fluctuation of

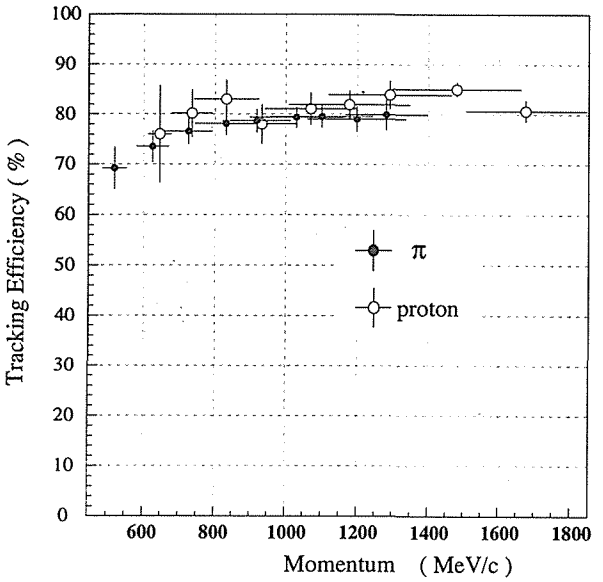

Fig. 25. Efficiencies of the track reconstruction. The particle identification of π^-'s (closed circle) and protons (open circle) was performed with the TOF data and combination of hit ID # of CH and FTOF. The vertical errors are statistical only. The horizontal errors represent the momentum resolution (r.m.s) obtained with combination of hit ID # of CH and FTOF (see the text and Fig.26).

about 5 % in the momentum range above 0.8 GeV/c. The reconstruction efficiency for pions were slightly lower than that for protons. It was consistent with the fraction of the pions which decayed in flight. Figure 26 shows methods of particle identification and momentum determination for the evaluation of track finding efficiency. Pions and protons were selected using the correlation between the hit positions on CH and FTOF as well as the TOF information as in the same manner as in the case of the second-level trigger. Those samples were fed to the track-finding/reconstruction algorithm to calculate the efficiency.

The mass of the particles was deduced from the results of the spline-fit and the TOF data. In order to reduce the deterioration of the timing due to the nuclear interaction in the FTOF counter or the accidental multi-particle hits, we applied a cut on the pulse height. Events were thrown away if the normalized pulse-height of the FTOF counter was 1.5 times as large as the mean value or larger. The reconstructed mass spectrum is shown in Fig.27. Particles in the reconstructed-mass range from 380 MeV/c^2 to 620 MeV/c^2 were chosen as K^+ candidates.

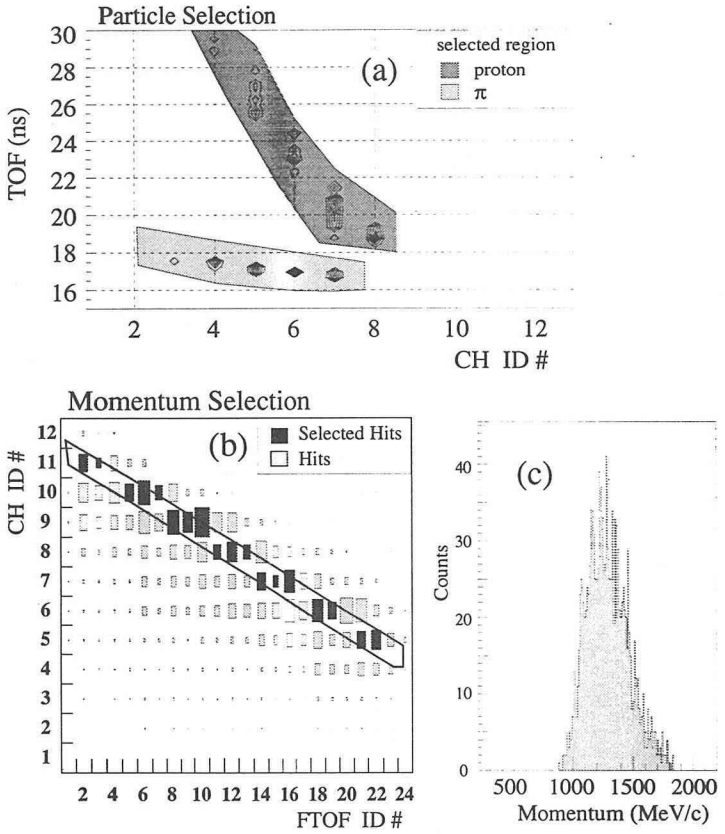

Fig. 26. Methods of particle identification and momentum determination of scattered particles for the evaluation of track finding efficency. (a) The particle identification of protons and pions was performed using the information of the hit patterns of CH and FTOF and also with the TOF data. The hatched areas represent the region for the selection of π^+'s and protons. (b) Momentum determination was made with the hit counter ID #'s of CH and FTOF. The momentum region obtained by selection of combination of hit ID # of CH and FTOF is shown in this figure. The momentum distribution of the events with the selected combinations is shown in (c).

Runge-Kutta Fitting and K^+ Selection

Finally, the momenta of the K^+ candidates were calculated by means of the Runge-Kutta integration method [43]. The momentum resolution was improved by factor 2 compared to the spline-fit. The initial parameters of each track were given by the quintic spline-fit. The particle trajectories were traced stepwise from 20 mm to 50 mm depending upon the derivative of the field strength of the spectrometer magnet. The iteration was continued until the reduced χ^2 increased from the value of the previous iteration, or it decreased less than 0.1 %. A typical number of iteration was 3.

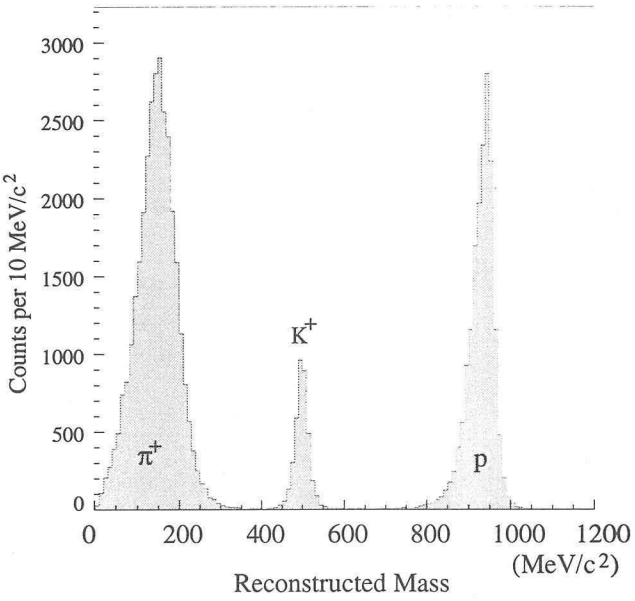

Fig. 27. Reconstructed mass distribution obtained with use of the results of the spline-fit. The shape of the reconstructed mass of protons was distorted due to the pre-selection procedure which rejected low-velocity particles.

The achieved momentum resolution was 0.5 % (r.m.s) for 1.2-GeV/c particles, which was limited by multiple scattering in the air and the materials in the spectrometer.

Using the track parameter obtained by the Runge-Kutta method, we tightened the requirement of the horizontal and vertical hit positions on FTOF. We took particles within the width of FTOF in horizontal and 40 mm in vertical which is 2.7 σ of the vertical position resolution of the FTOF. This requirement was effective to eliminate particles which decayed between the tracking chambers and FTOF. The mass of particles was re-evaluated. The reconstructed K^+ mass resolution was 18.5 MeV/c^2 (r.m.s) at 1.1 GeV/c. The mass range from 430 to 570 MeV/c^2 was selected. The π^+ contamination in the K^+ candidates was reduced to 0.2 %.

The vertex position was obtained using the beam track and the track of scattered particle. The distance between these tracks in the target volume were required to be less than 2 mm which corresponds to 3 σ of the track resolution. In the vertical direction, the scattered particle must be in a band with a width of $\pm$18 mm centered by the beam track. It was three times as large as the beam width (r.m.s).

The reconstruction efficiency of scattered particles was reduced by 9 % through the selection procedures after the spline-fit method. The selection on the pulse-height of FTOF counter was dominant process to reduce the efficiency.

3.1.3 Missing-Mass Spectrum of the (K^-,K^+) Reactions

The absolute values of the momenta of the beam particles and the scattered

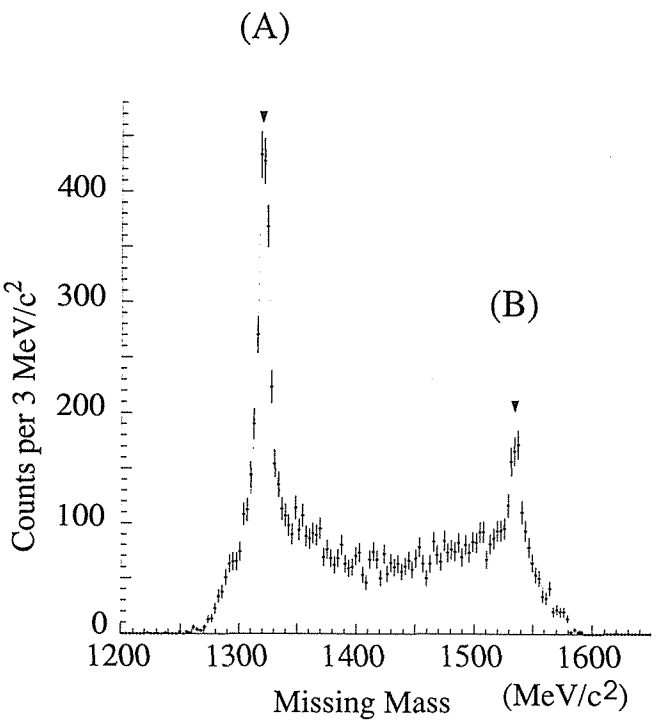

Fig. 28. Missing mass spectrum of the (K^-,K^+) reactions on the SCIFI-target (C-H). The interaction with a proton was assumed. The peaks correspond to the two-body production processes of A) Ξ^- and B) Ξ^{-*} ($\Xi(1530)^-$) on protons in the SCIFI-target.

particles were examined by the missing-mass spectrum of the (K^-, K^+) reactions shown in Fig.28. The spectrum is calculated assuming the reaction $K^- + p \rightarrow K^+ + X$. As shown in the figure, we identified the peaks corresponding to the productions of Ξ^-'s and Ξ^{-*}'s ($\Xi(1530)P_{13}^-$). We found also a clear peak of Σ^- in the missing-mass spectrum of (K^-, π^+) reactions (Fig.29). These spectra included the events on free protons and also on carbon nuclei in the SCIFI-target. The peaks corresponded to the events on the proton target, whereas the missing-mass for the events of the quasi-free scattering on the carbon were smeared out. The events in the region between the two peaks in Fig.28 correspond to reactions such as the two step process in carbon nuclei, $K^- + (N) \rightarrow \pi + Y$, then $\pi + (N) \rightarrow K^+ + Y'$, where (N) represents a nucleon in a carbon nucleus and Y and Y' denote hyperons with $S = -1$. The fitted value of the peak positions of the missing-mass was 1) Ξ^- : 1320.8 $\pm$ 0.2 $\pm$ 0.3 MeV/c^2, 2) Ξ^{-*} : 1535.3 $\pm$ 0.7 $\pm$ 0.3 MeV/c^2 and 3) Σ^- : 1197.3 $\pm$ 0.3 $\pm$ 0.4 MeV/c^2, where the second term for each value represents the statistical error and the third term is the systematic error due to the ambiguity of the fit function for the quasi-free process on the carbon target. These values agree well to the world averages of the mass values [39] ; 1)Ξ^- : 1321.32 $\pm$ 0.13 MeV/c^2, 2)Ξ^{-*} : 1535.0 $\pm$ 0.6 MeV/^{2} and 3)Σ^- : 1197.436 $\pm$ 0.033 MeV/c^2. The missing-mass resolution was

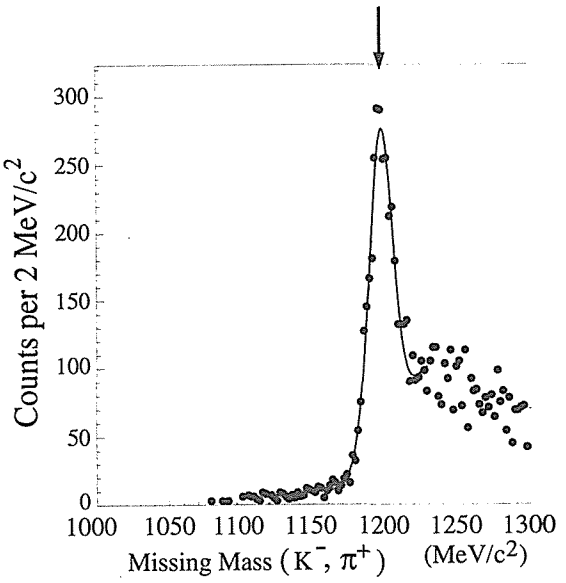

Fig. 29. Missing mass spectrum of (K^-, π^+) reactions on the SCIFI-target (C-H). The interaction with a free proton was assumed. The arrow represents the peak position obtained by fitting. The fitted line is shown by a solid line.

5.6 MeV/c^2 for the reaction $K^- + p \rightarrow K^+ + \Xi^-$.

3.1.4 Tagging Efficiency and Statistics

We obtained 19,669 candidates of the (K^-, K^+) reaction events with the first-level trigger and 13,538 candidates with the secodn-level trigger. The H production was studied in the K^+-momentum range above 0.95 GeV/c, although the quasi-free Ξ^- production was dominant. In this region, 6733 events were obtained. The obtained momentum spectrum of K^+ above 0.95 GeV/c is shown in Fig.30(a). It should be reminded that the chemical components of the SCIFI-target were carbon and hydrogen with the ratio of 1:1. The bump at about 1.1 GeV/c corresponds to the Ξ^- production on protons.

For the K^+ which reached the FTOF without decay in flight, the detection efficiency was evaluated to be about 55 % including the trigger efficiency. The total amount of K^- beam used in the analysis was 3.8×10^9 taking account of the efficiency of the trigger and detection rate in the offline analysis with the dead time correction.

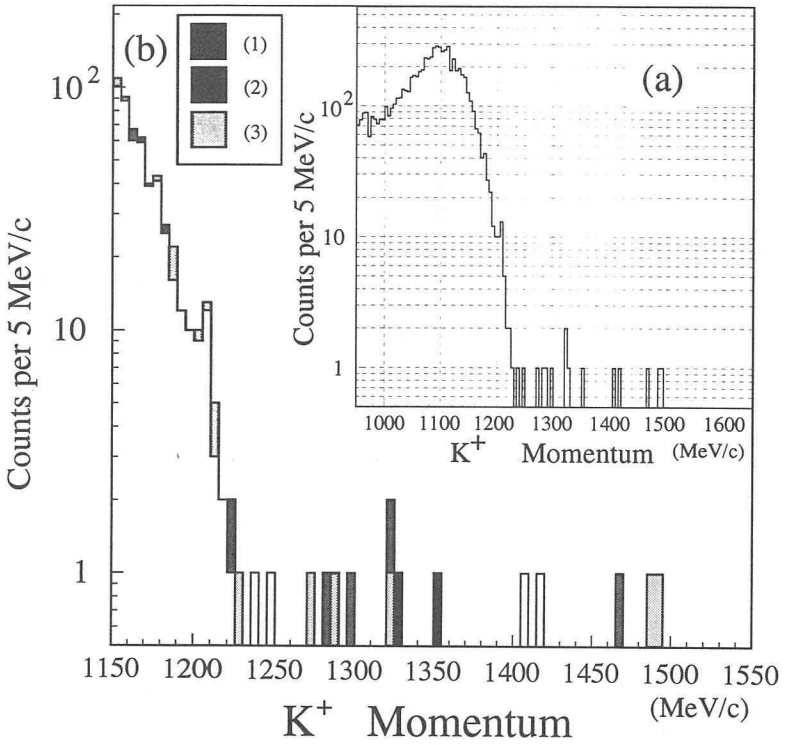

Fig. 30. (a) Momentum spectrum above 0.95 GeV/c of the K^+'s identified in the analysis of the data of the spectrometer, and (b) Momentum spectrum of the K^+ above 1150 MeV/c. The solid line represents the spectrum obtained in the analysis of the data of the spectrometer. The hatched areas represent the rejected events as background in the analysis of the data of the SCIFI-target. (1) Secondary interactions were observed as two or more kinks along the tracks of the beam and the scattered particles. (2) Events due to intermediate neutral particles. (3) Events with false tracks which were rejected by means of examination of the consistency between tracks predicted by the spectrometer and those detected in the SCIFI-target.

3.2 Analysis of (K^-,K^+) Events with SCIFI-Data

The pictures of the tracks in the SCIFI-target corresponding to (K^-,K^+) reactions were combined with the data of the spectrometer. The analysis of the SCIFI-target data was performed for the evnets in the K^+-momentum above 950 MeV/c where we searched for the H produced through the direct process. About 1.2 % of events which were remained after selections with the information from the beam line and spectrometer had been abandoned due to an error in the data acquisition of the SCIFI-data. The number of the pictures to be analyzed was 6621.

The data analysis for the SCIFI-target was performed in the following procedures; 1) calibration of the data and 2) checking the track of K^-'s and K^+'s in the SCIFI-data. The procedure 2) was of vital importance to remove the background events due to the secondary interactions and mis-tracking.

3.2.1 Calibration and Performance of the SCIFI-IIT System

The raw data of the SCIFI-target for one event consisted of thousands of pixel-data which corresponds to the pixels in the CCD cameras. The data for each pixel included 7-bits pulse-height (brightness) information and 19-bits data of the location of the pixel in the CCD chip. The pixel-data were converted to the position in the SCIFI-target to obtain one picture with the brightness information. Tracks in SCIFI-target were identified in the picture as sequential bright spots.

In the raw data, the image from the SCIFI-target was distorted due to the fringing field of the spectrometer magnet and the position dependence of magnification at the electrostatic focussing on the first stage of the IIT ("pin-hole distortion"). The distortion was calibrated using straight tracks of particles and also with an external light source which generated a test pattern. The distortion was calibrated within the accuracy of 200 μ m. The details of the calibration methods are found in Ref. [38,34].

One photon was recognized as a cluster pixels in the CCD having the size of about 180 μ m (r.m.s). The average number of detected photons for a minimum-ionizing-particles was about 0.55/mm along the track for each projection. The internal position resolution of one photon was about 290 μ m [27] (r.m.s). The resolution was limited mainly due to the size of the fiber and the accuracy of fiber packing.

3.2.2 Background Rejection of (K^-,K^+) Reaction using SCIFI Image-Data

We applied cuts on the (K^-,K^+) candidates using the SCIFI-data for the purpose of reducing false events whose tracks in the spectrometer system were recognized as K^+. In addition, this cut was useful to eliminate events in which the K^+'s were produced through secondary interactions. Here we performed scanning of the image data by human eyes in order to find the tracks which corresponded to the beam particles and the scattered particles.

Eye Scanning

We performed eye scanning for 6621 pictures using a screen-display. First, we removed pictures in which more than two interactions are overlapped accidentally (multiple exposure). This multiple exposure was due to the long decay time (2.4 μ sec) of the phosphor of the first stage of the IIT. The number of removed events was 15.

Secondly, we removed 28 events in which two or more kinks were observed along the trajectory (MK-type). These kinks corresponded to secondary interactions occured in the SCIFI-target. Since the probability of the nuclear interaction in the SCIFI-target was about 8 %, rejection of the K^+ produced in the secondary interaction was very important.

Thirdly, we eliminated events with K^+'s produced in the secondary interaction (N-Event) by neutral particles such as $\overline{K^0}$'s. There existed 57 events which had gap-spaces without image of trajectory between the incoming and the outgoing particles. Fig.31 shows a picture of typical event. The existence of the gap-space was confirmed both in the X and Y-projections of the SCIFI-data. Since the average number of photons along a track of a minimum-ionizing particle was about 5/cm, it was possible

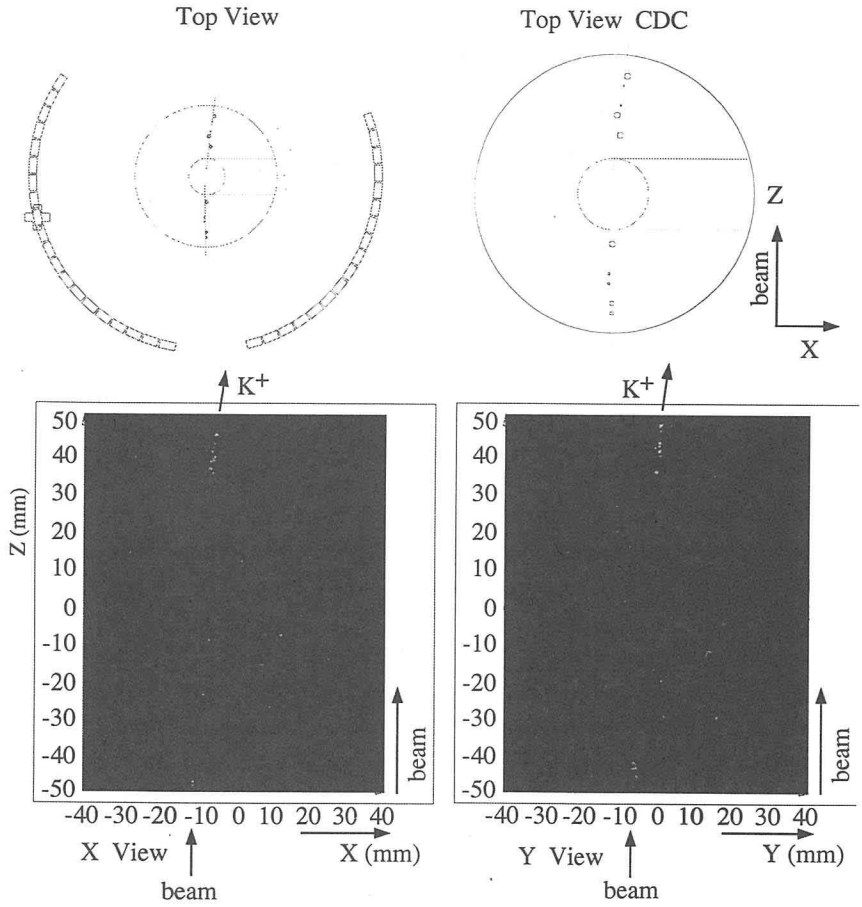

Fig. 31. A typical event due to an intermediate neutral particle (see the text). This event was mis-assigned as a (K^-,K^+) reaction with the K^+ momentum 1280 Mev/c by the analysis of the spectrometer system. The K^+ was produced in the secondary interaction of the intermediate neutral particle which was observed in the SCIFI-target.

to distinguish a neutral particle from a charged particle with the efficiency better than 98 % even if the pass length of the particle in the SCIFI-target was only 2 cm. The major source seems to be due to the K^-p charge exchange reaction followed by $\overline{K^0} - K^0$ conversion.

Finding of the Tracks of Beam and K^+ in the SCIFI-Target

Finding of the tracks of the beam and scattered particles in the data of the SCIFI-target was performed with a software program using the track parameters obtained from the data of the beam line and the spectrometer. There was an intersection between the predicted incoming tracks and outgoing track in both the X and Y-projections. A band along the predicted tracks of beam and scattered particles with a width of $\pm 3\,\sigma$ of the resoulutions was defined as the corridor. For convenience of tracking, the pictures were divided by the thickness of the fiber sheets. In each piece

of the divided pictures, the track information was shown as a bright photon cluster. In order to search for real tracks in the corridor, the cluster finding procedure was carried out. Fitting to a straight line was applied for the clusters of track candidates of the beam and of the scattered particles. We required the existence of the clusters for more than 1.5 cm continuously without brake. The efficiency for such track finding was obtained to be 97.5 % for the events categorized as good events by eye scanning.

In Fig.30(b), the momentum spectrum above 1150 MeV/c was shown for the events which were rejected in the analysis described above, i.e. 1) MK-type events, 2) N-type events and 3) false tracks. The number of the (K^-,K^+) candidates after these cuts was 6344.

4 Results and Discussion

The H production was searched for as a high-momentum K^+ in the region which is kinematically not allowed in the quasi-free Ξ^- production. Therefore, the H production results in the observation of an event with large missing-energy.

4.1 Missing-Energy Spectrum

To discriminate the candidates of the H production from the quasi-free Ξ^- production, we examined the spectrum of the missing-mass of the reaction $K^- + {}^{12}C \rightarrow K^+ + X$ (missing-energy). Figure 32 shows the missing-energy spectrum as a function of the binding energy of $\Xi^- + {}^{11}B$ system. In this figure, 0 MeV in the horizontal axis corresponds to the kinematical limit to produce Ξ^-'s in free space;i.e. $K^- + {}^{12}C \rightarrow K^+ + \Xi^- + {}^{11}B$. Consequently, the events above 0 MeV correspond to reactions such as the 2Λ, Ξ-hyper nucleus, or the H production. The missing-energy resolution was evaluated to be 9.5 MeV (r.m.s) by considering the momentum resolution of K^-'s and K^+'s.

4.2 Study of the H Candidates with SCIFI-Data

There are 15 events above -10 MeV in Fig.32. Table 6 shows the missing-energies, K^+ momenta and reconstructed masses of the K^+'s of these events. We investigated these events in the SCIFI-data to search for the signal of the H production.

There are two events with the missing-energy close to 200 MeV. An event has a momentum of the scattered particle of 1415.8 MeV/c (event-A), and the other has that of 1408.0 MeV/c (event-B). These two events would be explained as (K^-, π^+) reactions in which the π^+ was mis-identified as K^+, since the energy of the scattered particle corresponds the peak of the quasi-free Σ^- production. In the Σ^- production via (K^-, π^+) reaction, angular distribution of the π^+'s has a forward peak, and the averaged differential cross section in the acceptance is about 30 times as large as that of the Ξ^- production via (K^-,K^+) reactions [30]. The reconstructed mass resolution for π^+'s was about 70 MeV/c^2 in the π^+ momentum range from 1300 to 1450 MeV/c, and the reconstructed mass of the scattered particle of the latter

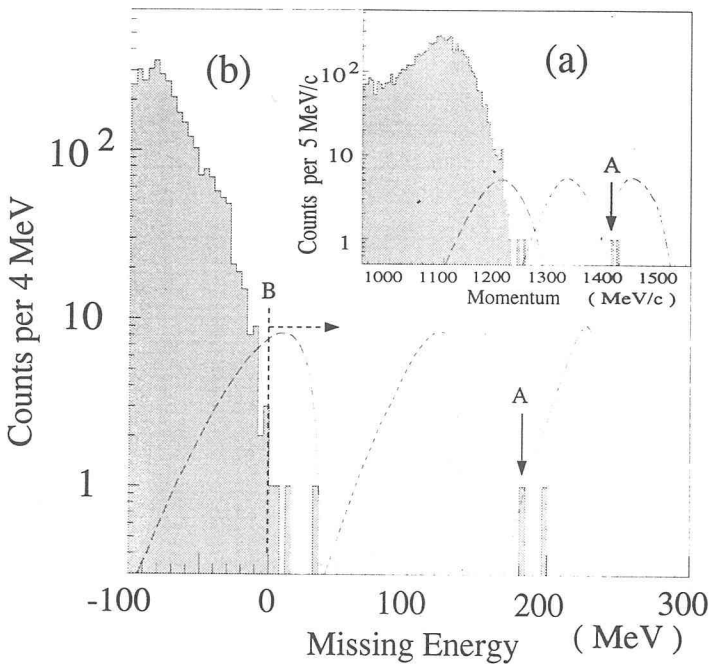

Fig. 32. (a) The K^+ momentum spectrum in the region of $p_{K^+} \geq 0.95$ GeV/c. The events which were rejected from (K^-,K^+) candidates in the analysis of the SCIFI-data were subtracted from Fig.30. (b) The missing-energy spectrum of (K^-,K^+) events above-100 MeV. The missing-energy was calculated as the reconstructed binding energy of Ξ^- in $^{12}_{\Xi}$Be. The line-B at 0 MeV corresponds to the kinematical limit of the free Ξ^- production, which is used as "cut-off" in the analysis (see the text). The events indicated by the arrow-A was rejected from (K^-,K^+) candidates in the analysis of the data of the SCIFI-target (see the text). The dashed, dotted and dash-dotted lines represent expected shapas of the spectra of the direct H productions with M_H = 2200, 2100 and 2000 MeV/c^2, respectively.

event is 4.1 σ apart from the mass of π^+. The corresponding background rate was 0.7 event in the K^+ momentum range from 1300 to 1450 MeV/c from the above considerations. Looking at the picture of the SCIFI-data, the event-A has the vertex position out of the fiducial area of the SCIFI-target. The event-B has a track of about 8 mm long from the vertex. Figure 33 shows the picture of the event-B. In this case, the momentum of Σ^- is sufficiently low to stop in the SCIFI-target, and this makes such a short track. The length of the short track in Fig.33 corresponds to the Σ^- of 284 $\pm$ 11 MeV/c, while the momentum of the Σ^- predicted from the spectrometer is 270 $\pm$ 10 MeV/c assuming that the reaction occurs on proton at rest. These values are consistent each other, and it supports the explanation that the event is Σ^- production via (K^-, π^+) reaction. Furthermore, the difference between the direction of the prong and the predicted momentum direction is so small as $0.02^{+0.11}_{-0.02}$ radian in the X-Z plane and $0.03^{+0.11}_{-0.03}$ radian in the Y-Z plane. It indicates that the

Table 6 The events which have residual energy above -10 MeV. B.E. is the energy in excess of the kinematical limit of the free Ξ^- production.

	B.E.(MeV)	p_{K^+} (MeV/c)	M_{K^+} (MeV/c^2)
1)	12.4	1212.8	468.9
2)	-8.4	1151.2	493.7
3)	-7.9	1187.1	505.0
4)	-2.0	1201.3	504.0
5)	1.6	1194.0	493.2
6)	183.8	1408.0	438.6
7)	5.6	1191.6	539.0
8)	197.4	1415.8	536.9
9)	-8.7	1176.9	465.4
10)	-1.5	1222.6	510.0
11)	-9.3	1217.2	531.7
12)	-9.7	1208.9	497.0
13)	35.8	1246.2	492.0
14)	-4.5	1181.9	523.0
15)	-0.9	1239.8	509.9

charged particle is produced on a free proton. Therefore, we rejected the event-B from the (K^-,K^+) candidates.

In the lower missing-energy region, there is one candidate which has a missing-energy of 35 MeV. The vertex is located out of the fiducial area of the SCIFI-data. There is no track which positively indicates the production of the H. The event might be the 2 Λ production or the hypernuclear production. It is possible to consider the event also as the background from (π^-,K^+) reaction due to the mis-identification of the π^- as K^-. The peak of the quasi-free Σ^- production process, $\pi^- + (p) \rightarrow \Sigma^- + K^+$, corresponds the K^+ momentum at about 1.25 GeV/c, and the background rate due to the reactions is obtained about 1 event taking account the mis-identification rate in the beam analysis.

The other 12 events have missing-energies close to the kinematical limit (0 MeV). There is a possibility of the coherent two-Λ production process $K^- + (pp) \rightarrow \Lambda + \Lambda + K^+$ or the Ξ^--hypernucleus production competing with the direct H production. We found 3 events which have tracks longer than 3 cm from the (K^-,K^+) reaction vertex. They are candidates for mesonic-decays of hypernuclei. The other 3 events have short tracks of about 1 cm long from the reaction vertices. One of them has additional two tracks forming the V-topology which seems to be the decay products of the Λ. The other 4 events have no clear tracks from the reaction vertex in which two events have tracks indicating the decay of Λ's. The two events remained have reaction vertices out of the fiducial area of the image-data. There is no positive candidate of the H production in the 12 candidates in the missing-energy range close to 0 MeV. They are candidates of coherent productions of double Λ's or Ξ^--hypernuclei. According to theoretical calculations [36, 37], several events of Ξ-hypernuclear productions are expected to be in this region close to the kinematical

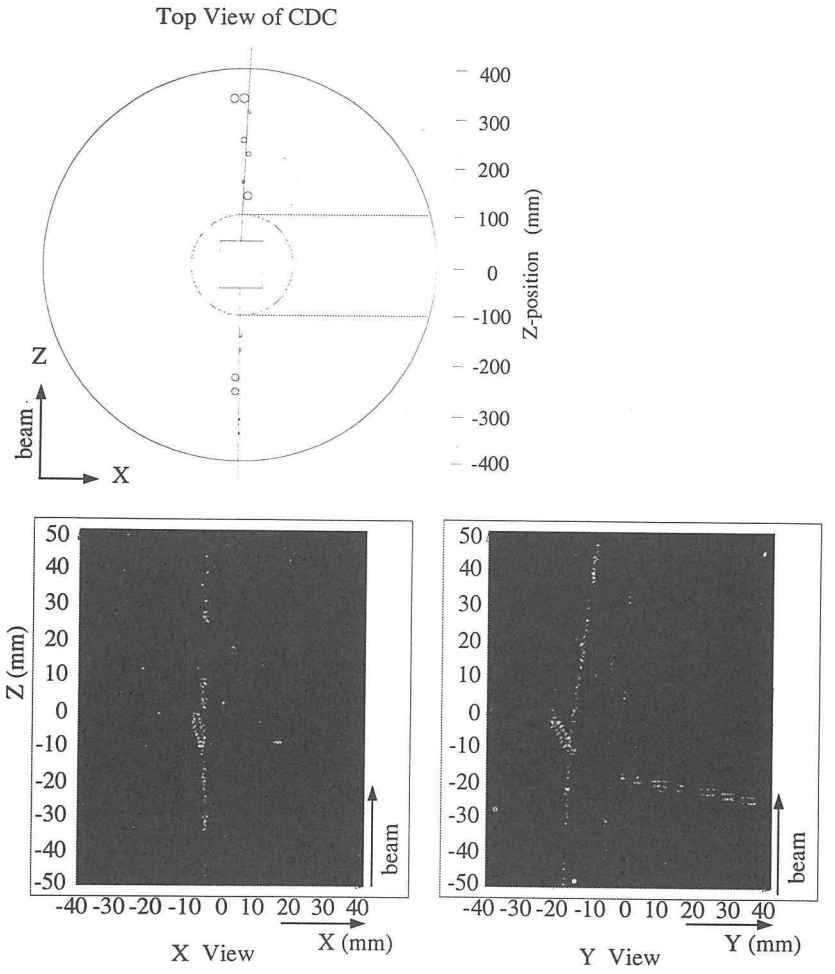

Fig. 33. A display of the event which was rejected from (K^-,K^+) candidates. The momentum and the reconstructed mass of the scattered particle are 1408 MeV/c and 438.6 MeV/c^2. The calculated missing-energy is 183.8 MeV. The event was assigned as Σ^- production in a (K^-, π^+) reaction on a free proton (see the text). The prong from the reaction vertex in the SCIFI-target corresponds to the Σ^- which stopped in the target.

limit.

There remained no positive candidate of the H in the remaining 14 events with missing energy larger than -10 MeV. These events are explained by other mechanisms than the H production. However, the production cross sections for the competing processes are not so clear. We, therefore, calculate the upper limit of the H production rate without subtraction of these events.

4.3 Upper Limits of the Production Cross-Section

In order to obtain the upper limit on the production cross-section, we calculated

the expected missing-energy spectrum in the H production. We used the same calculation method as that of Nakano [40] based on the scenario of Aerts and Dover [23]. The expected shape of the missing-energy is shown in Fig.32. In the calculation of the upper limit, we set a cut-off energy at 0 MeV in the missing-energy spectrum. In order to avoid the systematic error of the number of beam particles and the detection efficiency of the (K^-,K^+) reaction events, the upper limit for the ratio of the H production on the number of (K^-,K^+) reactions in the K^+-momentum range above 0.95 GeV/c (6344 events) was obtained. The production cross section was evaluated using the experimental data of E176[35] in which the nuclear dependence of the cross section of the (K^-,K^+) reactions[5] was measured.

The upper limit for the production rate of the H on the SCIFI-target normalized to the rate of the (K^-,K^+) reactions with the K^+ momentum above 0.95 GeV/c was calculated at 90-percent confidence level (UL) as :

$$UL = \frac{f(n)}{(\eta \times N_{(K^-,K^+)})}, \tag{8}$$

where $N_{(K^-,K^+)}$ is the number of (K^-,K^+) reactions in the K^+-momentum range above 0.95 GeV/c. The $f(n)$ is the upper limit for the Poisson distribution with "number of observed events" at 90-percent confidence level. The "number of observed events" is the number of detected events above the cut-off energy (0 MeV) having overlap with the calculated spectrum of missing-energy for the case of H production. The η is the detection efficiency of the H production in the missing-energy range above the cut-off. It is a function of the mass of H, since it depends upon the momentum of the K^+. We took into account the momentum dependence of the K^+-decay rate and of mass resolution of the detectors. In addition, the momentum dependence of the K^+ detection rate due to the trigger efficiency such as the survival rate against the online veto with the Čerenkov counter, SAC, was included in the η.

The obtained upper limits of the production rate of the H through the direct process on carbon target is shown in Fig.34 as a function of the mass of the H. Here, the upper limit was normalized to the rate of (K^-,K^+) reactions on C-H target with the K^+ momentum above 0.95 GeV/c. The axis on the right side of the figure shows the differential cross section of the H production on the carbon target at the forward scattering angle of the K^+ which is averaged in the acceptance mentioned before. The rapid increase of the upper limit of the H production with the mass around 2200 MeV/c^2 corresponds to the decrease of the detection efficiency of the H in the missing-energy range above the cut-off. The figure shows also the theoretically expected cross section of the H production calculated as in the same manner as Nakano [40] with the scenario of Aerts and Dover [23]. In the model of Arts and Dover, proton pairs in relative $^1S_0$ state in a nucleus contribute to produce the H. According to their original calculation for the H production cross section on the ^{3}He target, the

[5] The differential cross section of the (K^-,K^+) reactions averaged over the laboratory forward angular region between 1.7 degree and 13.6 degree is a) 99 $\pm$ 4 μb/sr for carbon target and b) 35 $\pm$ 4 μb/sr for proton target.

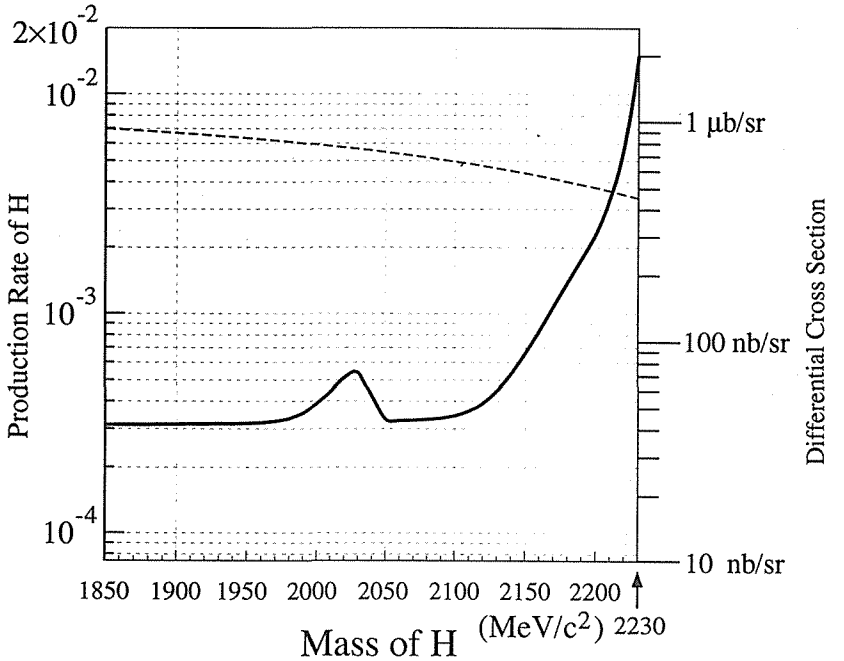

Fig. 34. The upper limit for the H production through the direct process. The solid line is the upper limit at 90-percent confidence level. The dashed line represents the theoretically expected production rate. The left axis represents the upper limit for the H production rate which is normalized to the rate of (K^-,K^+) reactions on C-H target with the K^+ momentum range above 0.95 GeV/c. The right axis represents the upper limit for the differential cross section of the H production in the (K^-,K^+) reactions on the carbon target at $P_K - = 1.66$ GeV/c, at 90-percent confidence level. The cross section was averaged in the acceptance of the K^+'s at the central production angle of 0 degree (see the text). The normalization error of ± 5% due to the ambiguity of the differentian cross section of the (K^-,K^+) reactions on a C-H traget is not included.

production rate of the H on ^{3}He is around 0.4 μ b/sr in the H mass range from 2050 to 2230 MeV/c^2. The production rate on ^{12}C is expected to be larger than that on ^{3}He, since the effective number of proton pairs in relative $^1S_0$ state in ^{12}C is about 4.7 [40]. The rate would be suppressed due to the absorption of K^- or K^+ in the target nucleus. The suppression factor is evaluated to be about 2.2 from the effective proton number of the (K^-, K^+) reaction on carbon which is about 2.9 for K^+ momentum above 0.95 GeV/c [35]. Hence, the production cross section of the H on ^{12}C is about twice as large as that on the ^{3}He target.

The present experiment has greatly improved the upper limit for the cross section of H production in the direct process. The upper limit of this experiment is lower than that of a previous experiment using an emulsion target (KEK-E176 [14]) by a factor of more than 5 in the mass range of the H from 1950 to 2150 MeV/c^2 due to

higher statistics with less background rate. For the H with the mass above 2150 MeV/c^2, the better momentum resolution of the K^- and K^+ enables us to obtain the upper limit of the H production for the first time. Furthermore, the effective number of the proton pairs in relative $^1S_0$ state for carbon target is five times as large as that of the Ag target [40]. Therefore, better sensitivity for the direct production of the H could be obtained with the SCIFI-target than in the case of the emulsion target, even in the case that the observed production rate would be the same. The present result of the upper limit is one order smaller than the theoretically expected rate for the H with the mass below 2140 MeV/c^2 and comparable at around 2210 MeV/c^2.

5 Conclusion

The H dibaryon was searched for by using a hybrid system of a high-resolution spectrometer and an active target comprising scintillating fibers with triggerable image-intensifier tubes as a track detector for the first time.

The experiment was performed using a 1.66-GeV/c separated K^- beam. The H dibaryon was searched through the direct production $K^- + {}^{12}\mathrm{C} \rightarrow K^+ + H + X$. A signature of the H production was the observation of a K^+ with momentum higher than that from the quasi-free Ξ^- production.

The total number of K^-'s was 3.8×10^9. The (K^-,K^+) reaction was identified with the spectrometer magnet, tracking chambers, Čerenkov counters and TOF hodoscopes. Backgrounds due to the secondary interactions have been reduced using the information of tracks in the scintillating-fiber target. We obtained about 6,300 events of (K^-,K^+) reactions with K^+ momenta above 0.95 GeV/c.

The missing-energy spectrum of the reaction $K^- + {}^{12}\mathrm{C} \rightarrow K^+ + X$ was investigated to find out an evidence of the H production through the direct production. There were 6 events above the kinematical limit of the quasi-free Ξ^- production. These events were examined in the image-data of the fiber target, and we found all these events could be explained as those of reactions such as hypernuclear productions. As the result, we did not find any positive candidates of the H-production events.

We obtained the upper limit for the cross-section of the H production in the direct process on carbon nuclei as 43 to 73 nb/sr at 90-percent confidence level for the mass range of the H from 1850 to 2150 MeV/c^2, which is one order as low as a theoretically expected rate and also the results of the previous experiment using an emulsion-counter-hybrid-system. The upper limit was obtained in the higher-mass region of the H up to 2230 MeV/c for the first time. The upper limit increases with the mass of the H from 80 nb/sr to 2 μb/sr around 2230 MeV/c^2. The sensitivity of the experiment to the H production in the mass range around 2210 MeV/c^2 was comparable with the production rate expected by Nakano using the calculation scheme of Aerts and Dover.

Finally, we would like to stress that the high momentum resolution with the spectrometer and powerful background reduction with the hybrid-system enabled us to obtain much higher sensitivity to the production of H through the direct process than

in the case of the previous experiments. We believe that such an experimental method will open new fields of particle and nuclear physics.

Acknowledgements

I would like to express my sincere gratitude to Prof. Akira Masaike. I am deeply grateful for his continuous supports, encouragements, guidance and introducing me to the particle and nuclear physics. I also would like to express my special gratitude to Prof. K.Imai, who is the spokesman of the KEK-PS E224 experiment, for his insightful advice and discussion on ideas for the experiment and on the physics of the *H* dibaryon. I wish to thank Prof. H. En'yo for exciting discussion and his great talent to solve problems with incredible speed which supported the experiment.

The experimental results described in this paper has been obtained with combined efforts of many individuals in the E224 collaboration. I would like to express my appreciation to all the members of the E224 collaboration. Especially I am indebted to Y.Itow, M.S.Chung, Dr.S.Aoki and Y.Goto for various discussion, online data acquisition and analysis of the data of the fiber target. I also wish to appreciate Y.D.Kim, J.K.Ahn and I.S.Park for their tireless studies on IIT and various type of fibers. I also gratefully appreciate to the collaborators who played a great role to design and construct the spectrometer. Among them, I would like to thank especially to Dr.M.Ieiri, H.Funahashi, M.Iinuma, N.Saito, Y.Matsuyama and M.Sekimoto. I would like to stress his special thanks to S.Mihara and Prof. P.Tlusty who deeply contribute to the operation and the analysis of the spectrometer. Thanks are also due to Prof. F.Takeuchi, Prof. K.S.Sim, Prof. Y.M.Shin, Dr. R.Takashima and Dr. I.Nomura for their guidance, discussion and valuable advice.

I am thankful to Dr. T.Iijima for his advice on the subject of the *H* particle. His contributions for the Čerenkov counters are also greatly appreciated. I also thank Prof. T.Fukuda for his helpful suggestions on the hypernuclear production. I appreciate Prof. Y.Akaishi, Prof. Y.Yamamoto, Prof. T.Motoba and Dr. S.Tadokoro who calculated the various rate of hypernuclear production.

This work was supported by staffs of KEK physics division, accelerator division and the beam handling division of proton synchrotron. Their continuous supports for the beam and magnet operation were strongly appreciated.

References

[1] R.L.Jaffe, Phys. Rev. Lett.**38** (1977) 195;**38** (1977) 617 (E).
[2] A.Th.M.Aerts, P.J.G.Mulders and J.J.de Swart, Phys. Rev. **D17** (1978) 260.
[3] K.F.Liu and C.W.Wong, Phys. Lett. **113B** (1982)1.
[4] P.J.G.Mulders and A.W.Thomas, J.Phys. G: Nucl. Phys. **9** (1983) 1159.
[5] B.O.Kerbikov, Yad, Fiz. **39** (1984) 816.
[6] S.Takeuchi and M.Oka, Phys. Rev. Lett. **66** (1991) 1271.
[7] M.Oka, K.Shimizu and K.Yazaki, Nucl. Phys. **A464** (1987) 700.
[8] B.Silvestre-Brac, J.Carbonell and C.Gignoux, Phys. Rev. **D36** (1987) 2083.
[9] U.Straub, Z.Zhang, K.Brauer, A.Faessler, S.B.Khadkikar and G.Lubeck, Nucl. Phy. **A508** (1990) 385c.

[10] P.B.Mackenzie and H.B.Thacker, Phys. Rev. Lett. **55** (1985) 2539.
[11] Y.Iwasaki, T.Yoshié and Y.Tsuboi, Phys. Rev. Lett. **60** (1988) 1371.
[12] A.S.Caroll et al., Phys. Rev. Lett. **41** (1978) 777.
[13] H.Ejiri et al., Phys. Lett. **B228** (1989) 24.
[14] S.Aoki et al., Phys. Rev. Lett. **65** (1990) 1729.
[15] S.Aoki et al, Prog. Theor. Phys. **85** (1991) 1287.
[16] B.O.Kerbikov, Sov.J.Nucl. Phys. **39** (1984) 516.
[17] M.Danysz et al., Nucl. Phys. **49** (1963) 121.
[18] D.Powse, Phys. Rev. Lett. **17** (1966) 782.
[19] K.Imai, Nucl. Phys. **A547** (1992) 199c-210c.
[20] B.Shahbazian, A.Kechechyan, A.Tarasov and A.Martynov, Z. Phys. **C39** (1988) 151.
[21] G.B.Franklin et al., AGS Research Proposal E813, BNL 1985, unpublished.
[22] P.D.Barnes, Nucl. Phys. **A547** (1992) 3c.
[23] A.T.M.Aerts and C.B.Dover, Phys. Rev. **D28** (1983) 450.
[24] A.T.M.Aerts and C.B.Dover, Phys. Rev. **D29** (1984) 433.
[25] J.K.Ahn, et al., Nucl. Phys. **A547** (1992) 211c-216c.
[26] J.K.Ahn, et al., Proceeding of HADRON93 (1993) (to be published).
[27] J.K.Ahn et al., Nucl. Instu. Meth. (to be submitted).
[28] Y.Itow, Master Thesis, Kyoto Univ. 1990, unpublished.
[29] Bellefon et al., Nuobo Cim., **A7** (1972) 567-72.
[30] D.F.Kane, Jr., Phys. Rev., **D5** (1972) 1583.
[31] A.Yamamoto et al., Nucl. Instr. Meth. **203** (1982) 35-43.
[32] K.Amako et al., Nucl. Instr. Meth. **197** (1982) 325-330.
[33] H.Boerner et al., DESY 80/27 (1980).
[34] Y.Itow, PhD thesis, Kyoto Univ. 1995, unpublished.
[35] T.Iijima et al., Nucl. Phys. **A546** (1992) 588.
[36] K.Ikeda et al., Prog. Theor. Phys. **91** (1994) 747.
[37] S.Tadokoro et al., INS-Rep. **1058** (1994) (preprint)
[38] M.S.Chung, PhD thesis, Korea Univ. 1995, unpublished.
[39] Particle Data Group, particle data (1994).
[40] T.Nakano, PhD thesis, Kyoto University, 1990, unpublished.
[41] T.Oosuka et al., KEK internal manual of TKO system.
[42] H.Wind Nucl. Instr. Meth. **115** (1974) 431-434.
[43] J.Myrheim and L.Bugge Nucl. Instr. Meth. **160** (1979) 43-48.